



HAL
open science

The Messinian Salinity Crisis deposits in the Balearic Promontory: an undeformed analog of the MSC Sicilian basins??

Fadl Raad, Johanna Lofi, Agnès Maillard, Athina Tzevahirtzian, Antonio Caruso

► **To cite this version:**

Fadl Raad, Johanna Lofi, Agnès Maillard, Athina Tzevahirtzian, Antonio Caruso. The Messinian Salinity Crisis deposits in the Balearic Promontory: an undeformed analog of the MSC Sicilian basins??. *Marine and Petroleum Geology*, In press, <10.1016/j.marpetgeo.2020.104777>. <hal-02977398>

HAL Id: hal-02977398

<https://hal.umontpellier.fr/hal-02977398v1>

Submitted on 24 Oct 2020

HAL is a multi-disciplinary open access archive for the deposit and dissemination of scientific research documents, whether they are published or not. The documents may come from teaching and research institutions in France or abroad, or from public or private research centers.

L'archive ouverte pluridisciplinaire **HAL**, est destinée au dépôt et à la diffusion de documents scientifiques de niveau recherche, publiés ou non, émanant des établissements d'enseignement et de recherche français ou étrangers, des laboratoires publics ou privés.



HAL Authorization

1 **The Messinian Salinity Crisis deposits in the Balearic Promontory: an**
2 **undeformed analog of the MSC Sicilian basins??**

3
4 **Fadl Raad¹, Johanna Lofi¹, Agnès Maillard², Athina Tzevahirtzian³, Antonio Caruso³**

5
6 ¹ Géosciences Montpellier, CNRS, Université de Montpellier, Université des Antilles - Bâtiment
7 22, Université de Montpellier 2, Place E. Bataillon, 34095 Montpellier Cedex 05, France

8 ² Géosciences Environnement Toulouse (GET), Observatoire Midi Pyrénées, Université de
9 Toulouse, CNRS, IRD, 14 avenue E. Belin, F-31400 Toulouse, France

10 ³ Dipartimento di Scienze della Terra e del Mare (DiSTeM), Università degli Studi di Palermo, Via
11 Archirafi 20-22, 90123 Palermo, Italy

12
13 **Correspondence**

14 Fadl Raad, Department of Geosciences Montpellier, France.

15 Email address: fadl.raad@umontpellier.fr

16 SaltGiant: www.saltgiant-etn.com

17
18 **Funding Information**

19 This research is carried out under the SALTGIANT ETN, a European project funded by the
20 European Union's Horizon 2020 research and innovation program under the Marie Skłodowska-
21 Curie grant agreement number 765256

22
23 **ABSTRACT**

24 The Messinian Salinity Crisis (MSC) is a controversial geological event that influenced the
25 Mediterranean Basin in the late Miocene leaving behind a widespread Salt Giant. Today, more
26 than 90% of the Messinian evaporitic deposits are located offshore, buried below the Plio-
27 Quaternary sediments and have thus been studied mainly by marine seismic reflection imaging.
28 Onshore-offshore records' comparisons and correlations should be considered a key approach
29 to progress in our understanding of the MSC.

30 This approach has however not been widely explored so far. Indeed, because of the erosion on
31 the Messinian continental shelves and slopes during the MSC, only few places in the
32 Mediterranean domain offers the opportunity to compare onshore and offshore records that
33 have been preserved from erosion. In this paper, we compare for the first time the MSC records
34 from two basins that were lying at intermediate water depths during the MSC and in which salt
35 layers emplaced in topographic lows: the Central Mallorca Depression (CMD) in the Balearic
36 Promontory, and the Caltanissetta Basin (CB) in Sicily. The reduced tectonic movements in the
37 CMD since the late Miocene (Messinian) till recent days, favored the conservation of most of
38 the MSC records in a configuration relatively close to their original configuration, thus allowing
39 a comparison with the reference records outcropping in Sicily. We perform seismic
40 interpretation of a wide seismic reflection dataset in the study area with the aim of refining the
41 mapping of the Messinian units covering the Balearic Promontory (BP) and restituting their
42 depositional history based on a detailed comparison with the Messinian evaporitic units of the
43 Sicilian Caltanissetta Basin. We discuss how this history matches with the existing 3-stages
44 chrono-stratigraphic model. We show that the Messinian units of Central Mallorca Depression
45 could be an undeformed analog of those outcropping on-land in the Sicilian Caltanissetta Basin,
46 thus questioning the contemporaneous onset of the salt deposition on the Mediterranean
47 scale. We show a change in seismic facies at a certain range of depth between stage 1 MSC
48 units, and wonder if this could reflect the threshold/maximum depth of deposition of bottom
49 growth PLG selenites passing more distally to pelagic snowfall cumulate gypsum. Moreover, we
50 confirm that PLG could be deposited in water depths exceeding 200m.

51

52 **KEYWORDS**

53 Messinian Salinity Crisis, Balearic Promontory, Central Mallorca Depression, Caltanissetta Basin,
54 Outcrops.

55

56

57

58

59

60

61 1 Introduction: Messinian Salinity Crisis and Intermediate Basins

62 The Messinian Salinity Crisis (MSC) is a prominent and still misunderstood event that influenced
63 the Mediterranean Basin in the late Miocene, leaving behind a Salt Giant with a volume of
64 about $1.2 \times 10^6 \text{ km}^3$ (Ryan, 1976; Haq et al., 2020) deposited in a relatively short time interval of
65 $\sim 0.64 \text{ Ma}$ (Krijgsman et al., 1999a,b; CIESM, 2008; Manzi et al, 2013). The first studies dedicated
66 to the MSC took place onshore (Selli, 1960) while offshore works (Ryan et al., 1971) followed
67 the first scientific drillings of the deep-sea drilling project DSDP (Hsu et al., 1973b). Since then
68 and until today, numerous studies have been conducted in order to better understand the
69 series of events that modified the basin during the Messinian and, despite these efforts, most
70 of the controversies still persist (see review in Roveri et al., 2014a). A consensus model for the
71 MSC was proposed after the CIESM publication in 2008, inspired from the 2 stage model of
72 Clauzon et al. (1996), where the MSC has been divided in 3 stages:

73 - stage 1 (from 5.97 to 5.60Ma, i.e. $\sim 370 \text{ ky}$): this stage marks the MSC onset, where the
74 lowermost primary evaporites were deposited in shallow water basins.

75 -stage 2 (from 5.60 to 5.55Ma, i.e. $\sim 50 \text{ ky}$): at this stage, salt bodies (mainly halite) were
76 deposited in deep basins accompanying the maximum sea-level drawdown (of debated
77 amplitude). Shallower basins evaporites underwent erosion and reworked evaporites were
78 deposited.

79 -stage 3 (from 5.55 to 5.33Ma, i.e. $\sim 220 \text{ ky}$): this stage was later on divided into 2 sub-stages,
80 stage 3.1 (from 5.65 to 5.42), in which upper evaporites were emplaced and stage 3.2 (from
81 5.42 to 5.33), that is known also as Lago Mare stage, where sediments with brackish water
82 fauna content were deposited.

83 This model has been widely built based on onshore studies performed on several key peri-
84 Mediterranean outcrops among which the ones from Sicily. This model has recently been
85 challenged at least for the Eastern Mediterranean Basins by studies from recent oil industry
86 offshore drillings (e.g. Meilijson et al., 2019).

87 Today, more than 90% of the MSC evaporites are lying offshore (Fig. 1A; Ryan et al., 2009; Lofi
88 et al., 2011a, b; Lofi, 2018). Offshore drillings remain very limited (DSDP and ODP drillings and
89 oil industry wells) and the offshore MSC records thus still largely un-sampled. The most efficient
90 approach in the offshore domain remains the seismic reflection method.

91 There is an agreement about the important role of the pre-MSC topography on the distribution
92 of the MSC sediments, although paleo-geographic reconstructions are still not well constrained
93 (Masclé and Masclé, 2019). In their review, Roveri et al., (2014a) proposed a schematic
94 classification of the Messinian sub-basins in the Mediterranean, where they differentiate
95 shallow (0–200 m water depth), intermediate (i.e. relatively deep-water, 200–1000m) and deep
96 basins (water depth > 1000m). In this view, these sub-basins are thought to be physically
97 disconnected from each other by topographic sills, and hold specific MSC records.

98 The shallow marginal basins have been largely studied onland as they are outcropping in areas
99 tectonically active during and/or after the MSC (e.g. Southeastern Spain, Apennines, Piedmont).

100 The Messinian sedimentary record in these basins is nevertheless always incomplete because it
101 has been exposed to erosion during the MSC sea level fall and/or due to tectonics. The main
102 feature in the onshore outcrops is the presence of thick gypsum beds that mark the onset of
103 the MSC (e.g. Yesares member in Sorbas Basin (Krijgsman et al., 2001); Vena del Gesso
104 formation in the Northern Apennines (Vai and Lucchi, 1997); Cattolica Gypsum group in the
105 central Sicilian Basin (Decima and Wezel, 1971)). They are called Primary Lower Gypsum (PLG),
106 corresponding to MSC stage 1 and are usually interpreted as precession driven beds (Lugli et al.
107 2010). A few studies have also recognized the presence of PLG in the offshore domain (e.g.
108 Northern Adriatic Sea (Ghielmi et al., 2013); Balearic Promontory (Ochoa et al., 2015)).

109 The deep MSC basins are only observed offshore and they contain salt sequences > 1 km thick
110 (see review in Lofi et al., 2011a, 2011b; Lofi, 2018). In the Western Mediterranean, the Algero-
111 Provencal Basin is known to contain the full MSC sedimentary sequence or the so-called trilogy
112 (Montadert et al., 1970).

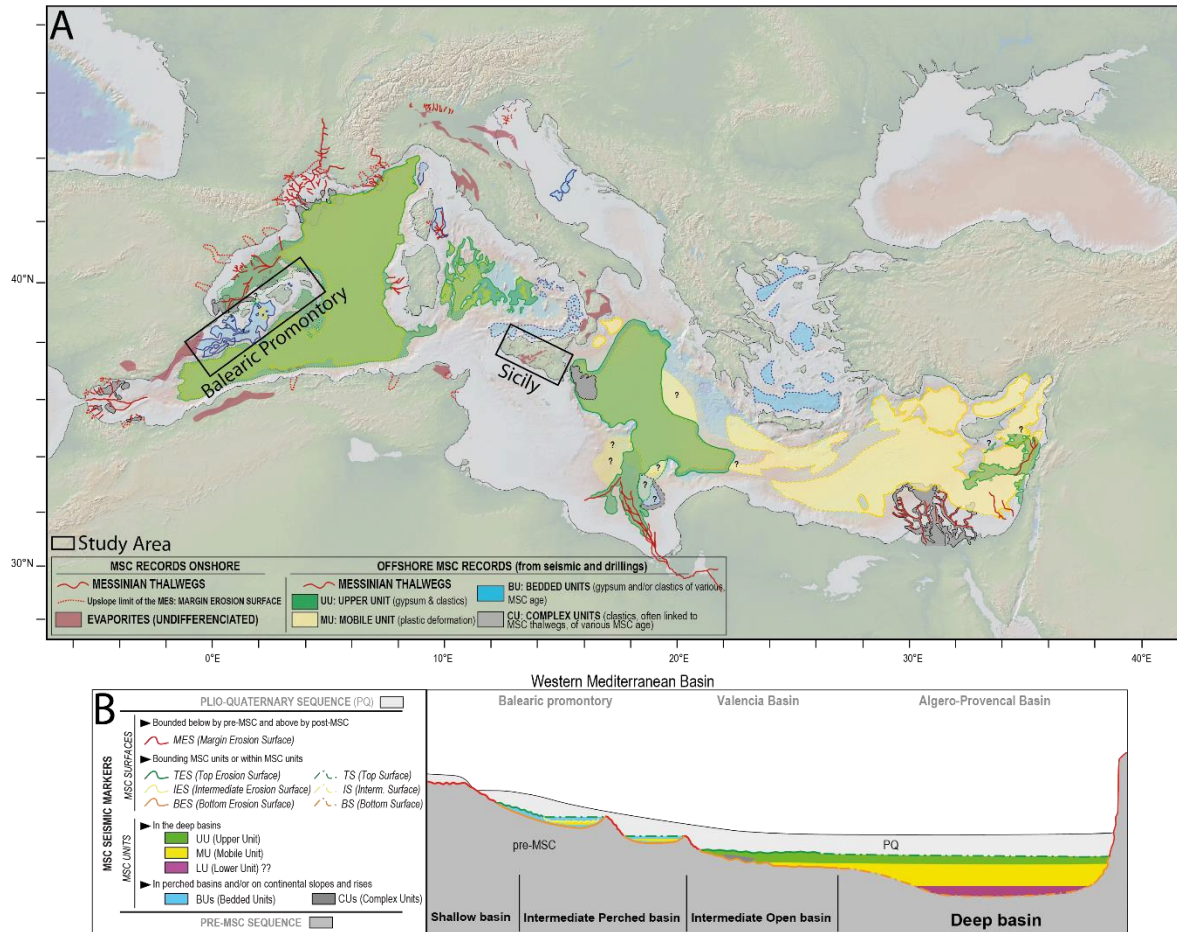
113 Following the nomenclature of Lofi et al. (2011), the 3 main seismic units forming this deep
114 basin succession are: 1- the lower unit (LU), never sampled; 2- the mobile unit (MU), thought to
115 be mainly made of Halite based on its transparent seismic facies and plastic deformation; 3- the

116 upper unit (UU) which uppermost part is made of clastic sediments, dolomitic marls, clastic
117 gypsum and anhydrite (Hsu et al., 1973a). The deep basin trilogy of the western Mediterranean
118 Basin has never been drilled except for its topmost part, and thus lacks chronostratigraphic and
119 lithostratigraphic control. The MSC record in the eastern Mediterranean (Levant Basin) differs
120 from the trilogy described in the western basin (Lofi et al., 2011a, b; Lofi, 2018) as it consists of
121 up to 2km thick halitic MU with distinct internal reflection packages (Bertoni and Catwright,
122 2006; Feng et al., 2016; Meilijson et al., 2019), overlain by a thin UU (Gvritzman et al., 2017;
123 Madof et al., 2019) made of clastic rich anhydrite that has been recently drilled (Gvritzman et
124 al., 2017).

125 The intermediate basins are lying between the shallow and deep basins (e.g. Cyprus and
126 Caltanissetta Basins). The MSC record in these basins differs from the one described in shallow
127 (containing mainly PLG) and deep (thick salt layer) basins, and can contain various deposits: 1-
128 euxinic shales/dolostones of stage 1 that are considered the later distal equivalent of the PLG
129 (e.g. Piedmont Basin (Dela Pierre et al., 2011)), 2- Resedimented Lower Gypsum RLG of stage 2
130 (e.g. Sicily (Roveri et al., 2006)) and 3- Upper Evaporites UE of stage 3 (e.g. Cyprus (Manzi et al.,
131 2016)).

132 When lying offshore today, intermediate basins can also contain various seismic units that are
133 Messinian in age, including 1- bedded units (BU) (e.g. Balearic promontory (Driussi et al., 2015;
134 Maillard et al., 2014); Adriatic Basin (Ghielmi et al., 2013); Eastern Corsica Basin (Thinon et al.,
135 2016)), 2- a relatively thin salt layer (e.g. Balearic Promontory (Maillard et al., 2014)), and 3- an
136 UU (e.g. Valencia Basin (Maillard et al., 2006)) lying above a Complex Unit (CU) (Valencia Basin
137 (Cameselle and Urgeles, 2017)).

138 In this work, we consider as intermediate any basin that during the MSC was lying deeper than
139 marginal basins (~200m water depth) and shallower than the deep basins, containing either
140 none of the deep basin MSC trilogy members or only some of them (Fig. 1B).



141
 142 **Figure 1.** A: Extension map of the MSC seismic units around the Mediterranean illustrating our study area
 143 (modified from Lofi, 2018). Relief map is taken from Geomapapp (www.geomapapp.org). B: schematic present-day
 144 cross section of the Western Mediterranean basin. It shows a conceptual present-day distribution of the MSC
 145 offshore markers along a transect from shallow into deep basin passing through the intermediate basin (salt
 146 tectonics and post MSC movements are not included) (modified from Lofi, 2018).

147
 148
 149 Some or part of the intermediate basins are outcropping nowadays (e.g. Sicily and Mesaoria
 150 Basins) and are thus considered as key areas to provide a stratigraphic link between marginal
 151 and deep basins. Offshore intermediate basins have not been intensively studied so far,
 152 although they may permit a comparison with some key onshore outcrops. Another importance
 153 of the offshore intermediate basins is that they may contain sedimentary records that are
 154 missing in the onshore outcrops that have undergone post-MSC erosion.
 155 In this paper, we compare two basins that are thought to be lying at intermediate depths
 156 during the MSC and in which salt layers are encountered: the Central Mallorca Depression

157 (CMD) on the Balearic Promontory (Maillard et al., 2014), and the Caltanissetta Basin (CB) in
158 Sicily (Roveri et al., 2014b). The first one is lying offshore between Ibiza and Mallorca islands, in
159 a passive tectonic setting, and is studied via seismic profiles. The second one is lying onshore in
160 an active tectonic context, and its outcrops have been studied widely as references for
161 understanding the MSC. First, we present a detailed study of the seismic records of the CMD.
162 We then discuss similarities, in terms of geometry, facies, distribution and thickness between
163 the Messinian deposits in both basins and we tempt to demonstrate that the CMD may be
164 considered as an undeformed analog of the Sicilian CB. Finally, we propose a depositional
165 scenario for the CMD and discuss the implications of the observations on the MSC event.

166

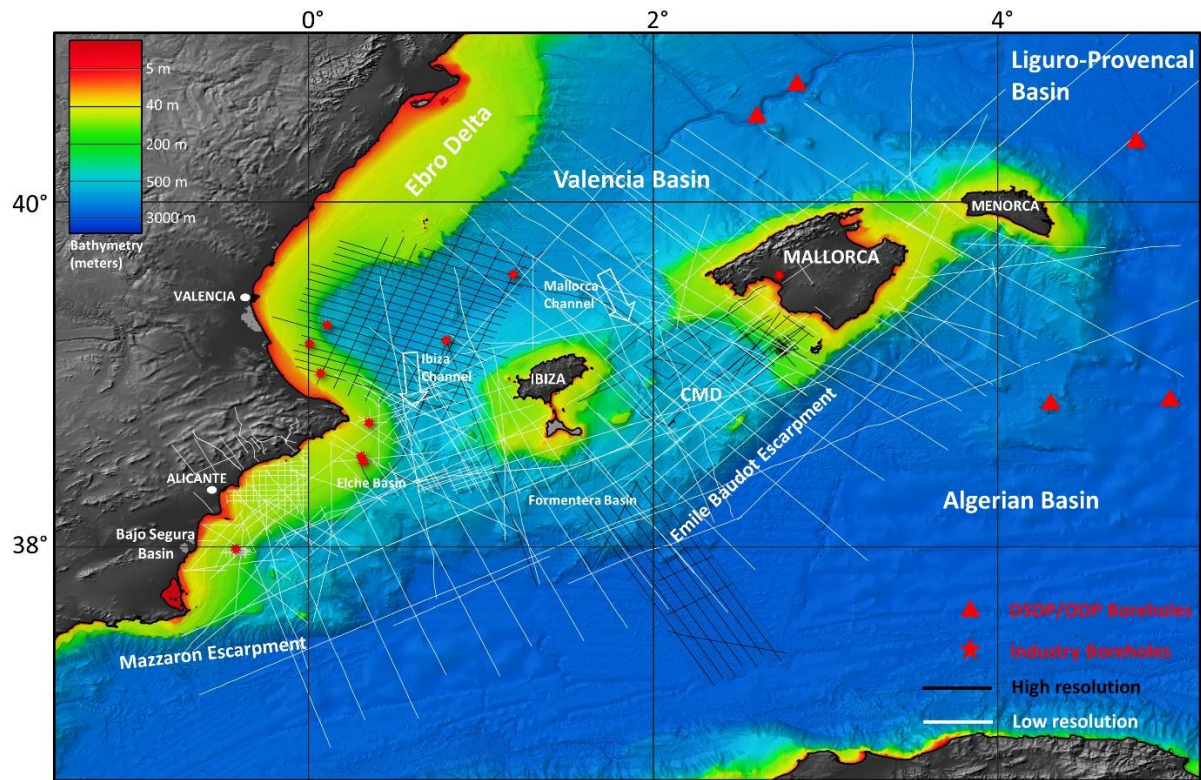
167

168 2 Geological background of the study areas

169 2.1 The Balearic Promontory: Tectonics, Architecture and Messinian Salinity Crisis

170 Surrounded by 2 deeper basins, the Balearic Promontory (BP) is a continental high that includes
171 the Balearic Islands. It is made of 2 main morphologic blocks (Acosta et al., 2002): the Mallorca-
172 Menorca block and the Ibiza-Formentera block (Fig. 2). The two blocks are separated by an
173 elliptical depression, approximately 1050m water deep, called the Central Mallorca Depression
174 (CMD). To the south, the BP is delimited by 2 steep escarpments marking the border with the
175 Algero-Provencal deep Basin (>2400m depth): the Mazarron and Emile Baudot Escarpments,
176 separated by the Ibiza Channel that, with the Mallorca Channel, connects the BP to the Valencia
177 Basin (>1200m depth) (Fig. 2).

178



179
 180 **Figure 2.** Bathymetric map showing the seismic dataset used for this study. CMD= Central Mallorca Depression.
 181 Bathymetry is downloaded from the European Marine Observation and Data network (EMODnet) database
 182 available online (www.emodnet-bathymetry.eu). White thick arrows indicate marine channels. Boreholes shown in
 183 the map represent a set of both industrial (IGME) and exploratory drillings (ODP and DSDP). Onshore digital
 184 elevation model has been produced using Copernicus data and information funded by the European Union- EU-
 185 DEM layers (www.eea.europa.eu).
 186
 187

188 The BP is known to be the north-eastern prolongation of the compressional Betic Cordillera
 189 thrust system (Roca, 2001). It is thought that the compression started in the late Oligocene to
 190 the south and then prolonged further to the north during the Burdigalian (Gelabert et al.,
 191 1992; Sabat et al., 2011), while the surrounding Valencia and Algerian Basins underwent rifting
 192 in the back-arc context of the retreating Apennines-Maghrebian subduction. From late
 193 Serravallian and up to recent times, the BP underwent mild post-orogenic extension, resulting
 194 in a NE-SW normal fault system expressed plainly by the Palma Graben in Mallorca (Roca and
 195 Guimera, 1992; Sabat et al., 2011).

196 This tectonic evolution of the BP thus resulted in a very complex structure including highs and
 197 lows resulting from compression and extension. The present-day BP contains a series of

198 perched sub-basins lying at different depths, stepped from the present-day coastline near
199 Alicante (Spain) down to the deep basin (Fig. 3A, B). Most of these sub-basins were probably
200 already existing during the Messinian and inherited their structure from the tectonic evolution
201 of the promontory. Today they are forming a series of topographic lows (Fig. 3B), more or less
202 connected, lying at various water depths (Driussi et al., 2015). During the MSC, these lows have
203 been filled with deposits up to 500m thick (Maillard et al., 2014; Driussi et al., 2015; Ochoa et
204 al., 2015).

205

206 2.1.1 MSC in the surrounding deep basins

207

208 South of the BP, the MSC record in the Algerian Basin is represented by the deep basin trilogy
209 ie. LU, MU and UU (Lofi et al., 2011a, b; Lofi, 2018). The UU and MU pinch out on the Mazarron
210 and Emile Baudot escarpments (Camerlenghi et al., 2009) and they show no connection with
211 the MSC units of the BP (Figs. 3A and 4A). North-East of the BP, in the Provencal Basin, the MSC
212 trilogy is also present (Montadert et al., 1970; Lofi et al., 2005). Towards the Valencia Basin, the
213 LU and MU thin out progressively and pinch out in the area where a volcanic ridge separates
214 the Provencal from the Valencia Basin (Fig. 3A; Maillard and Mauffret, 2006; Maillard et al.,
215 2006; Pellen et al., 2019). The UU extends into the Valencia Basin, thinning out from the NE to
216 the SW where it pinches out and passes into a Margin Erosional Surface (MES) on the
217 Catalan/Ebro Margins and volcanic structures (Maillard et al., 2006; Urgeles et al., 2011),
218 whereas towards the east it drapes the lower margin of the BP (Driussi et al., 2015) and it
219 passes into a MES. In the western extremity of this basin, Comeselle et al. (2017) evidenced the
220 existence of a widespread CU unconformably overlain by, here very thin, UU (Fig. 3A). They
221 interpreted the CU as mass transport deposits resulting from large-scale destabilization of the
222 continental slope during the initial rapid sea-level drawdown and exposure of the shelf and
223 upper slope. Other CU exist locally at the downslope mouth of Messinian valleys (Maillard et al.,
224 2006)

225 Recently, Pellen et al. (2019) interpreted an additional MSC unit (unit SU12) lying below the
226 MES on the Ebro Margin, and below the LU in the Valencia and Provencal Basins, which is

227 thought to have been deposited during the MSC base-level fall. Maillard et al. (2006) proposed
228 that following this important base level drop, the Valencia Basin was subaerially exposed and a
229 widespread erosion surface was created (Bottom Erosional Surface, BES). The UU successively
230 was emplaced under shallow water during a relative rise in base level as attested by their
231 aggrading and onlapping geometry (Lofi et al., 2011a, b). An erosional surface at the top of the
232 UU (Top Erosional Surface, TES) could be a result of dilution during the Lago-Mare phase,
233 possibly associated to a base level drop preceding the Zanclean reflooding (Escutia and
234 Maldonado , 1992; Maillard et al., 2006). For Camesselle and Urgeles (2017) this erosion is
235 minor and can be found only locally due to the dilution during the Lago Mare event.

236

237

238 2.1.2 MSC in the Balearic Promontory:

239 Several studies showed the presence of a thin MSC unit offshore the BP, disconnected from the
240 other MSC units in the surrounding basins (Maillard et al., 2014; Driussi et al., 2015; Ochoa et
241 al., 2015). Based on seismic profile interpretation, Driussi et al. (2015) identified a “MSC unit”
242 (Table 1) extending all over the BP (their figure 4) from the present-day coastline down to the
243 deepest part in the Formentera Basin (~1750m). This seismic unit is characterized by 2 to 7 sub-
244 parallel continuous reflections of medium amplitude. It locally includes an internal facies made
245 up of very thin reflections (Ft) with lower amplitude, found usually at the top of the MSC unit.
246 The “MSC unit” is locally lying on an erosional unconformity (BES) and is eroded at the top (TES)
247 towards the borders of the CMD.

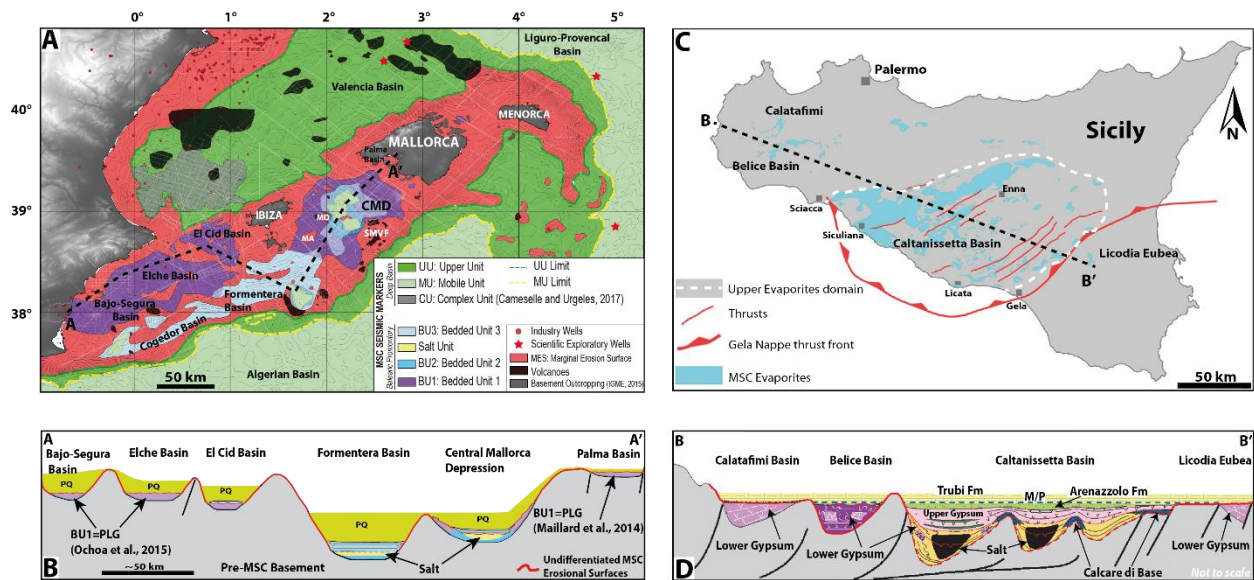
248 Several works then proposed that this “MSC unit” is made of several sub-units and that not all
249 of them have the same MSC age, depending on their location on the promontory (Maillard et
250 al., 2014; Ochoa et al., 2015; Roveri et al., 2019).

251 Ochoa et al. (2015), based on borehole cuttings and logs tied to high-resolution seismic
252 reflection profiles, demonstrated that the “MSC unit”, which they called Bedded Unit (BU,
253 sensu Lofi et al., 2011a, b) (Table 1), in Elche and Bajo Segura sub-basins corresponds to the PLG
254 (Fig. 3B; see also their figures 2 and 8). This PLG is equivalent to the first stage evaporites found
255 onland, for example in the Sorbas and Bajo Segura Basins (Soria et al., 2008) or in the Palma

256 Basin boreholes (Fig. 4A; Baron and Gonzalez, 1985; Rosell et al., 1998; Maillard et al., 2014;
257 Garcia-Veigas et al., 2018). In this area, the seismic facies of the PLG consists of sub-parallel
258 continuous 2 to 7 reflectors forming a Bedded Unit (BU), with very strong acoustic impedance
259 at the base and at the top (see their figure 8). It is clearly cut by the TES, whereas no erosion is
260 identified at the bottom. Based on their results, these authors suggested that PLG gypsum
261 precipitation and/or preservation could occur in non-silled basins at water depth exceeding
262 200m. Both Ochoa et al. (2015) and Driussi et al. (2015) questioned the connectivity between
263 the different shallow sub-basins (e.g. Bajo Segura and Elche Basins) and the ones currently lying
264 deeper, because of the presence of local structural highs separating them, and because the
265 density of seismic profiles is not high enough to show the connectivity. More recently, Roveri et
266 al. (2019) hypothesized that only the shallower domains of the Elche and Bajo Segura sub-
267 basins contained PLG, with the deeper parts of these basins located beyond some volcanic sills
268 containing Resedimented Lower Gypsum (RLG) (their figure 14 a, b). However, no data support
269 their new interpretation and mapping. At the present time, it is thus not clear whether the BUs
270 filling the sub-basins lying deeper correspond to PLG, RLG or another MSC deposit.

271 In a study dedicated to the CMD, Maillard et al. (2014) distinguished two different sub-units
272 within the MSC unit of Driussi et al. (2015) (see their figure 7): 1- a Slope Unit (SU) located
273 clearly on the Mallorca and Ibiza slopes and 2- a Bedded Unit (BU) lying deeper and containing a
274 thin salt unit (Table 1). The authors discussed the possible chrono-stratigraphic models for
275 those 2 MSC units in the CMD (see their figure 12). They question whether the SU, being older
276 than the BU, could be synchronous or could post-date the emplacement of the PLG of the
277 Palma Basin. Based on low-resolution high-penetrative seismic profiles, Maillard et al. (2014)
278 also argued that the salt layer in the CMD might be thicker than what is observed on the high-
279 resolution seismic lines. Another salt unit is recognized in the southernmost part of Formentera
280 sub-basin (Fig. 3A, B and Fig. 5D; Driussi et al., 2015). It is lying on a present-day depth of
281 ~450m below seafloor, whereas the salt in the CMD lies on 520m below seafloor.

282



283
 284 **Figure 3.** A: Map showing the present-day extent of the MSC units in the Balearic Promontory (BP) and the
 285 surrounding deep basins. Light grey lines are isochrones (every 200ms TWTT) of the offshore depth of the base
 286 Plio-Quaternary unit. Black dotted line shows the position of the section shown in 3B. Thin white lines in the
 287 background are the positions of the seismic profiles used for the interpretation. MA=Mount Auzias; MO=Mount
 288 Oliva; SMVF=South Mallorca Volcanic Field; CMD=Central Mallorca Depression. Note that on the BP salt units are
 289 present in different perched basins (CMD, Cogedor Basin and Formentera Basin) lying at different depths. Notice
 290 also that bedded unit (BU1) extension in Elche and Bajo Segura basins is more important than what has been
 291 mapped by Driussi et al. (2015). B: Schematic profile across the perched basins of the BP showing the present day
 292 setting of the different bedded and salt units overlain by the PQ unit; the colors of the MSC units are the same
 293 used in 3A's legend. The pre-MSC basement was drawn from the compilation and mapping of the Base Messinian
 294 horizon from the seismic dataset. Black dotted line shows the position of the section shown in 3D. PQ= Pliocene-
 295 Quaternary unit. C: Simplified map of the extent of the MSC evaporitic sediments in the different Sicilian basins
 296 (modified from Caruso et al., 2015). D: Schematic geological cross section across the Sicilian MSC basins showing
 297 the settings of the evaporitic units filling the sub basins topped by the base Pliocene Trubi sediments (modified
 298 from Roveri et al., 2006). Notice how in both the BP and Sicilian basins, the different sedimentary units belonging
 299 to the MSC are contained in a series of sub-basins lying at different depths with only the deepest basins containing
 300 salt.

301
 302
 303
 304

305 Onland Mallorca, the MSC record is expressed by the Santanyi limestones, that represent the
 306 Terminal Carbonate Complex (TCC), made of carbonatic microbialites, oolites and marls (Mas
 307 and Fornos, 2012). These authors suggest that the TCC is the lateral time equivalent of the PLG
 308 drilled in the bay of Palma. None of the boreholes drilled onland Mallorca records the TCC and

309 PLG together (Baron and Gonzalez, 1985), which supports this interpretation. Overlying the
310 TCC, and below the lower Pliocene sediments, a lacustrine-continental sedimentary unit known
311 as the Ses Olles Formation that contains brackish to fresh water faunal assemblages, thus
312 interpreted as representing the Lago Mare episode (Mas and Fornos, 2013). According to these
313 authors the Lago Mare unit is cut by an erosional surface created during the major base-level
314 drawdown, suggesting that the Lago Mare phase is related here to stage 1 of the MSC. This is
315 not in agreement with the current crono-stratigraphic model (CIESM, 2008; Roveri et al.,
316 2014a).

317

318

319

320

321 Onland Ibiza, Late Miocene units outcrop only locally and show common characteristics with
322 units known in Mallorca, such as the reef complex or a unit interpreted as the TCC (Durand-
323 Delga et al., 1993; Pomar et al., 1996; Lezin et al., 2017). Important continentalization episode
324 has been recently identified on top of these units with erosion and karstification, paleosols and
325 gravity-driven instabilities that are thought to record the major sea-level fall (Odonne et al.,
326 2019; Maillard et al., 2020).

327

328

329

330

331 2.2 The Sicilian Central Caltanissetta Basin: Geological context and MSC

332 Unlike the BP, the Sicilian Basins have been very active tectonically since the MSC.

333 Belonging to the Central Mediterranean domain, Sicily's structural and geological evolutions
334 derive from the convergence between the African continental margin and the Eurasian plate
335 (Catalano et al., 2013; Henriquet et al., 2020).

336 During the lower Miocene, the SE-wards shift of the Calabrian accretionary wedge above the

337 slab, including ALKaPeCa blocks (i.e. Alboran, Kabylies, Peloritani, Calabria; Bouillin, 1986), lead
338 to the growth of the Sicilian collisional complex (Catalano et al., 1996). The latter corresponds
339 to a well-exposed fold-and-thrust belt (FTB) (Albanese and Sulli, 2012), the Maghreb-Apennine
340 thrust belt, crossing from east to west the Sicily Island with the Gela Nappe along the thrust
341 front (Lickorish et al., 1999).

342 The Caltanissetta Basin, located in the arcuate part of the Gela Nappe (Fig. 3C), represents the
343 main foredeep of the frontal thrust belt system (Butler et al., 1997). It consists of a single thrust
344 sheet and comprises a series of continuously tightening folds (Lickorish et al., 1999). Its late
345 Neogene evolution is related to the opening of the Tyrrhenian Sea (Kastens et al., 1988). The CB
346 is organized in an alternation of depocenters and highs that are mostly related to active
347 thrusting synclines (Grasso and Butler, 1991; Butler et al., 1995; Catalano et al., 2013).

348 During the MSC, evaporites including halite were deposited in the CB and are mostly
349 outcropping today, which made it a reference basin for the study of the MSC event. A complete
350 sequence has been also found in a great number of cores in the CB, where the sequences are
351 schematically formed of Tripoli Formation (30-90m), Calcare di base alternated to primary
352 selenitic gypsum (> 300 m), halite and kainite (~ 500m) and Upper Gypsum (100-200m) (Rouchy
353 and Caruso, 2006; Caruso et al., 2015). This tripartite character of the MSC sequence recalls the
354 deep basin trilogy, thus the MSC succession of the central Sicilian CB was initially assimilated to
355 an uplifted part of the deep basin succession, although not necessarily as the deepest areas
356 (Decima and Wezel, 1971; Garcia-Veigas et al., 1995; Hsü et al., 1978; Rouchy, 1982a; Rouchy
357 and Saint Martin, 1992; Schreiber, 1978; Clauzon et al., 1996; Rouchy and Caruso, 2006).

358 However, different opinions exist about the marginal vs. deep basinal character of Sicily during
359 the Messinian (Clauzon et al., 1996, 2005; Krijgsman et al., 1999a,b; Butler et al., 1995) which
360 resulted in a number of chrono-stratigraphic models and related MSC scenarios (Fig. 4 E-G; e.g.
361 Decima and Wezel 1971; Garcia Veigas et al., 1995; Butler et al., 1995; Rouchy and Caruso
362 2006; Roveri et al., 2008). Recently, some authors classified the CB as an intermediate basin
363 with a complex stratigraphy as a result of its growth on an orogenic wedge (Roveri et al., 2008;
364 Roveri et al., 2014b).

365

366 According to the mentioned works, the MSC deposits in CB (Fig. 4D) can be summarized as
367 follows:

368 - Lower Evaporites (LE) or Lower Gypsum (LG) (Decima and Wezel, 1973): this unit is
369 made of massive bedded gypsum intercalated with clay beds with a thickness up to
370 140m (Lugli et al., 2010). Roveri et al. (2006) divided this unit into primary PLG and
371 resedimented RLG. The PLG consists of thick selenitic gypsum beds that vary from large
372 massive selenites to gypsarenites, separated by thinner organic-rich shale horizons. The
373 change in facies inside each cycle is thought to reflect the passage from arid to humid
374 phase at the insolation minima and the insolation maxima respectively at a precessional
375 scale (Lugli et al., 2010). The PLG in the Sicilian MSC basins (Fig. 6A-C) records the same
376 cyclicity (up to 13 cycles; Fig. 6C) as other PLG found in other marginal basins such as
377 Sorbas Basin and the northern Apennines. According to Lugli et al. (2010) the cyclicity
378 encountered in the PLG reflects the paleo-depositional environment, suggesting a
379 general shallowing-upward trend with a change in the general hydrology of the basin.
380 Moreover, these authors state that in the Sicilian Basins, PLG is found exclusively in
381 silled shallow basins (<200m depth) at the borders of the main foredeep depression and
382 has been deposited during stage 1 of the MSC (CIESM, 2008), whereas the lateral
383 equivalent of the PLG in the deeper parts of the basins is represented by levels of marls,
384 diatomites and thin laminated dolostone (calcare di base 2, see next paragraph) ~20m
385 thick (Manzi et al., 2011). The base of the PLG unit is conformable with pre-MSC
386 deposits, whereas its top is cut by an erosional surface (Fig. 6A-C).

387 The RLG, bounded by the regional MES at the bottom (Roveri et al., 2008), is found in
388 the main foredeep. It consists of resedimented gypsum that varies from huge and
389 undeformed PLG blocks to gypsarenites and gypsum laminates that has been re-
390 deposited during stage 2 of the MSC. There is a controversy of whether the origin of the
391 RLG is related to the combination of salt deformation followed by collapse dissolution
392 (Rouchy and Caruso, 2006) or due to sub-aqueous gravity flows in the foredeep due to
393 erosion or thrusting of large PLG masses (Roveri et al., 2008).

394

- 395 - Calcare di Base (CdB): this unit is made of complex carbonate formation with different
396 facies (Decima et al., 1988; Rouchy and Caruso, 2006; Ziegenbald et al., 2010) that are
397 found most commonly on structural highs separating perched basins. The most
398 widespread facies are m-thick micritic limestones (calcite and/or aragonite) of
399 evaporative and/or bacterial origin, often found as brecciated deposits and interbedded
400 with shales and clastic gypsum (Caruso et al., 2015; Perri et al., 2017). The CdB shows
401 common unfossiliferous and evaporitic character marked by halite and gypsum
402 pseudomorphs (Ogniben, 1957; Pedley and Maniscalco, 1999), which suggest a shallow
403 depositional environment close to the coastline (Suc et al., 1995a; Butler et al., 1999).
404 However, the origin and the position of the carbonates belonging to the CdB is still very
405 highly debated. Caruso et al. (2015) consider the CdB as the lateral equivalent to the
406 PLG, slightly diachronous, thus formed during stage 1 of the MSC. These authors argue
407 that the transition from the pre-MSC sediments (Tripoli Formation) to the CdB is
408 continuous without any evident unconformity and they relate the brecciation process
409 observed to local collapses with limited transport.
- 410 On the other hand, Manzi et al. (2011) divided the CdB into 3 different types, with only
411 type 2 (primary dolomitic limestones) belonging to the first stage of the MSC. Whereas
412 CdB types 1 and 3 belong to the second stage of the MSC, with type 1 formed as the
413 diagenetic product of bacterial sulfate reduction (BSR) of original clastic gypsum in
414 presence of hydrocarbons, and type 3 made of brecciated limestones that formed due
415 to regional mass transports.
- 416
- 417 - Salt: this unit is made mainly of halite and even large amounts of K-Mg salts and it is
418 found mainly in the central CB (Fig. 4D), where its thickness reaches 400-600m at the
419 Realmonte mine (Decima and Wezel, 1971, 1973; Lugli et al., 1999). There, it shows a
420 clear shallowing upward trend until reaching an exposure surface (Figs. 4E-G and 7B)
421 expressed by ~1.5m desiccation cracks (Lugli et al., 1999), which suggest that the salt
422 deposition started in a deep stratified water body that experienced a drawdown until
423 the subaerial exposure and truncation (Schreiber et al., 1976; Lugli et al., 1999). It is also

424 characterized by a very high frequency halite-clay cyclicity (cm to dm thick) that has
425 been correlated to Quasi-Biennial Oscillation, the El Nino Southern Oscillation, the
426 sunspot number solar cycle and lunisolar tidal cycle (Manzi et al., 2012). The precession
427 cycles of the deep basin salt of the eastern Mediterranean suggested by Manzi et al.
428 (2018) and more recently by Meilijson et al. (2019) have not been observed in the salts
429 of the CB.

430

431 - Upper gypsum (UG) or Upper evaporites (UE): like the salt, this unit is present mainly in
432 the CB (Fig. 4D) where it can reach thicknesses up to 300m. The most complete section
433 outcrops at Eraclea Minoa along the south-western coast of Sicily (Fig. 8C). It is made of
434 a rhythmic alternation of clays and marls interbedded with sandy and fine grained
435 carbonates and seven gypsum bodies made by multiple strata of finely-laminated
436 gypsum (balatino) and gypsarenites/selenites (Caruso and Rouchy, 2006; Grossi et al.,
437 2015).

438 The chrono-stratigraphic tuning of the UE differs between the different authors. Rouchy
439 and Caruso (2006) recognized 6 precession-driven sedimentary cycles, with a possible
440 7th basal cycle, represented by a deformed gypsum deposit overlaid by the Arenazzolo
441 sandstones (see next paragraph, Arenazzolo member). The Arenazzolo/Trubi contact
442 marks the Messinian/Zanclean boundary (GSSP at Scala dei Turchi - Eraclea Minoa) and
443 the return to normal marine conditions (Van Couvering et al., 2000; Pierre et al., 2006).
444 Whereas Manzi et al. (2009) interpreted nine to ten sedimentary cycles, including the
445 Arenazzolo member. According to these authors, each one of the cycles reflects
446 oscillations in the basin's base level and its water concentration associated to transitions
447 from wet to dry environments, marked by an erosional surface at the end of each cycle.
448 However, there is a disagreement about whether these oscillations started with brackish
449 conditions (e.g. Decima and Wezel, 1971) or with marine conditions (e.g. Rouchy, 1976)
450 and then evolved to hyperhaline conditions. For Rosell et al. (1998) the primary selenitic
451 crystals on the top of each cycles reflect marine conditions, whereas Butler et al. (1995)
452 considered them as salt-lake deposits. Londeix et al. (2007) suggested that the pollen

453 content of the clay layer, preceding the last gypsum bed of the different cycles at
454 Eraclea Minoa, indicates variable conditions that vary from distal to coastal. The base of
455 the UE is marked by an unconformity (Decima and Wezel, 1973; Butler et al., 1995;
456 Garcia-Veigas et al., 1995). The UE lie on the salt in the distal part of the basin, whereas
457 towards the proximal parts it shows onlap terminations on the underlying unit (ie. LE
458 and/or CdB), where the terrigenous content decreases and becomes enriched in coarser
459 material, due to changes in the fluvial discharge and drainage (Roveri et al., 2008).

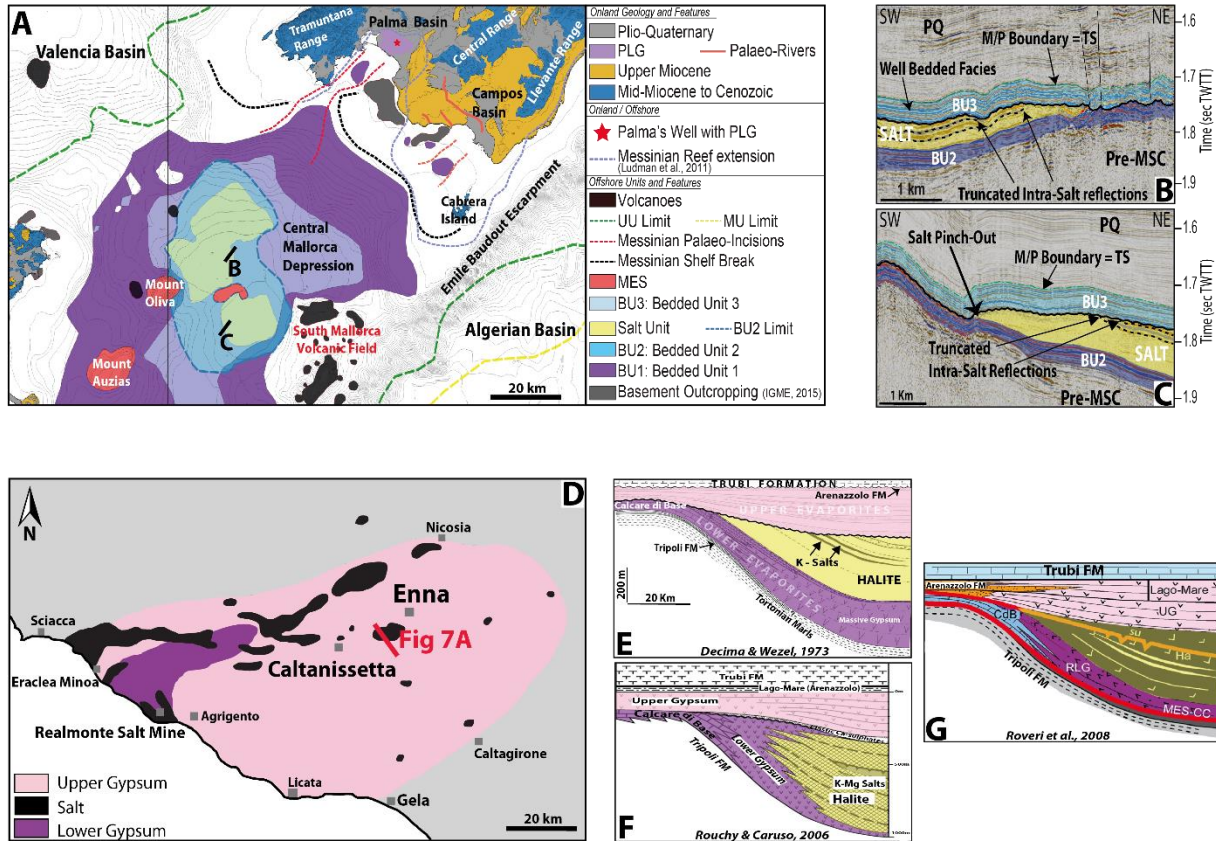
460

461 - Arenazzolo member: this unit overlays the UE and is topped by the Pliocene marking the
462 Messinian/Zanclean contact. It comprises a stratified arkosic sand with alternating thin
463 layers of different grain-size which yielded a well-diversified fauna corresponding to
464 brackish-water ostracods species (Lago Mare), mostly of Paratethyan origin (Bonaduce
465 and Sgarrella, 1999; Rouchy and Caruso, 2006). Some authors distinguished the Lago
466 Mare unit from the Arenazzolo member with the later lying unconformably on the
467 earlier (Cita and Colombo, 1979; Bache et al., 2012). According to these authors there is
468 a transition in the depositional environment from brackish shallow-water conditions
469 during the Lago Mare to a high-energy littoral environment. Above the Arenazzolo lies
470 unconformably the Trubi Formation that reflects open deep-water condition as shown
471 by foraminiferal fauna (Cita and Colombo, 1979; Pierre et al., 2006) and dinoflagellate
472 cyst flora (Londeix et al., 1999; Londeix et al., 2007). Bache et al. (2012) suggested a 2
473 step reflooding after the MSC acme in order to explain these transitions.

474

475 In this paper, for our comparison with the CMD record, we will be focusing mainly on the
476 Caltanissetta Basin where most of the stratigraphic models of the MSC are based on (Fig. 4). In
477 particular we will consider the geometries, facies, distribution and thickness of the MSC units.

478



479
 480 **Figure 4.** A: Detailed map of the MSC units and features in the Central Mallorca Depression (CMD). Note how the
 481 salt in the depocenter of the depression is distributed in 2 patches separated by a local topographic high. Isobaths
 482 (every 50m) represent the present-day bathymetry. Onland geology mapping of south Mallorca and North Ibiza is
 483 modified from geological map of Spain 1:50000 (IGME). Volcanoes and outcropping basement are from the
 484 geological map of Spain 1:1000000. BU1-PLG unit in the Palma Basin is mapped after Maillard et al. (2014). B-C:
 485 Parts of seismic profiles illustrating the geometrical relationship between the MSC units in the CMD: they show
 486 how the salt is lying between two MSC bedded units (BU2 and BU3) and contains internal reflections truncated at
 487 the top by an erosional surface. D: Map showing the distribution of the evaporitic units in CB (modified from
 488 Caruso et al., 2015). E-G: Sedimentary models showing the settings and geometrical relationships of the MSC
 489 evaporites in the CB published by different authors since the beginning of the studies of the MSC in that area
 490 (modified from Decima and Wezel, 1973; Rouchy and Caruso, 2006, Roveri et al., 2008). Note how in both study
 491 areas the settings and the geometrical relationships between the sedimentary units are similar, where we have a
 492 salt unit eroded at the top and sandwiched between two other units belonging to the MSC.

493
 494
 495

496 3 Data and Methods:

497 In this study we use a series of 2-D seismic reflection profiles covering the whole BP area with
498 the highest density of data in the CMD compared to the other sub-basins (Fig. 2). Part of this
499 dataset consists of low-resolution seismic lines including old oil industry data that has been
500 recently re-processed, provided by Spectrum Company, with a standard processing flow until
501 pre-stack time migration. Other old non-reprocessed seismic data was also provided by the
502 Instituto Geologico y Minero de Espana (IGME). The high-resolution seismic lines are mainly
503 covering the CMD and have been acquired during the SIMBAD survey (Maillard and Gaullier,
504 2013). High- and low-resolution lines were crossed for a better recognition, interpretation and
505 mapping of the MSC units and surfaces.

506 The interpretation of the profiles was performed using the software Petrel® by Schlumberger®.
507 Analysis of the seismic profiles following a seismic stratigraphic procedure in terms of reflection
508 terminations, erosional truncations, onlaps, downalps and configurations, allowed the
509 identification of seismic units and their boundaries (Mitchum and Vail, 1977). The seismic
510 horizons were then exported in digital format and imported to the geographic information
511 system QGIS for the mapping of the MSC markers.

512 For the MSC seismic units and surfaces we adopt the nomenclature proposed by Lofi et al.
513 (2011a, b).

514 The mean acoustic velocities used for the time-depth conversion and thickness estimates are:
515 1500 m/s for the seawater; 2300 m/s for the Pliocene-Quaternary sequence derived from
516 detailed curves based on wells (Maillard et al., 2014; Driussi et al., 2015 and references
517 therein); 4500 m/s for the MSC pre-halitic unit (bedded units BU1 and BU2), based on the sonic
518 log data tied to seismic profiles from Ochoa et al. (2015); 4780 m/s for the salt unit, based on
519 laboratory measurements done on samples of halite from the MSC salts from Sicily published
520 by Samperi et al. (2020); 3500 m/s for the MSC post-halitic bedded unit (BU3) assuming that it
521 contains more terrigenous sediments than the pre-halitic bedded units (see results and
522 discussion for more details).

523

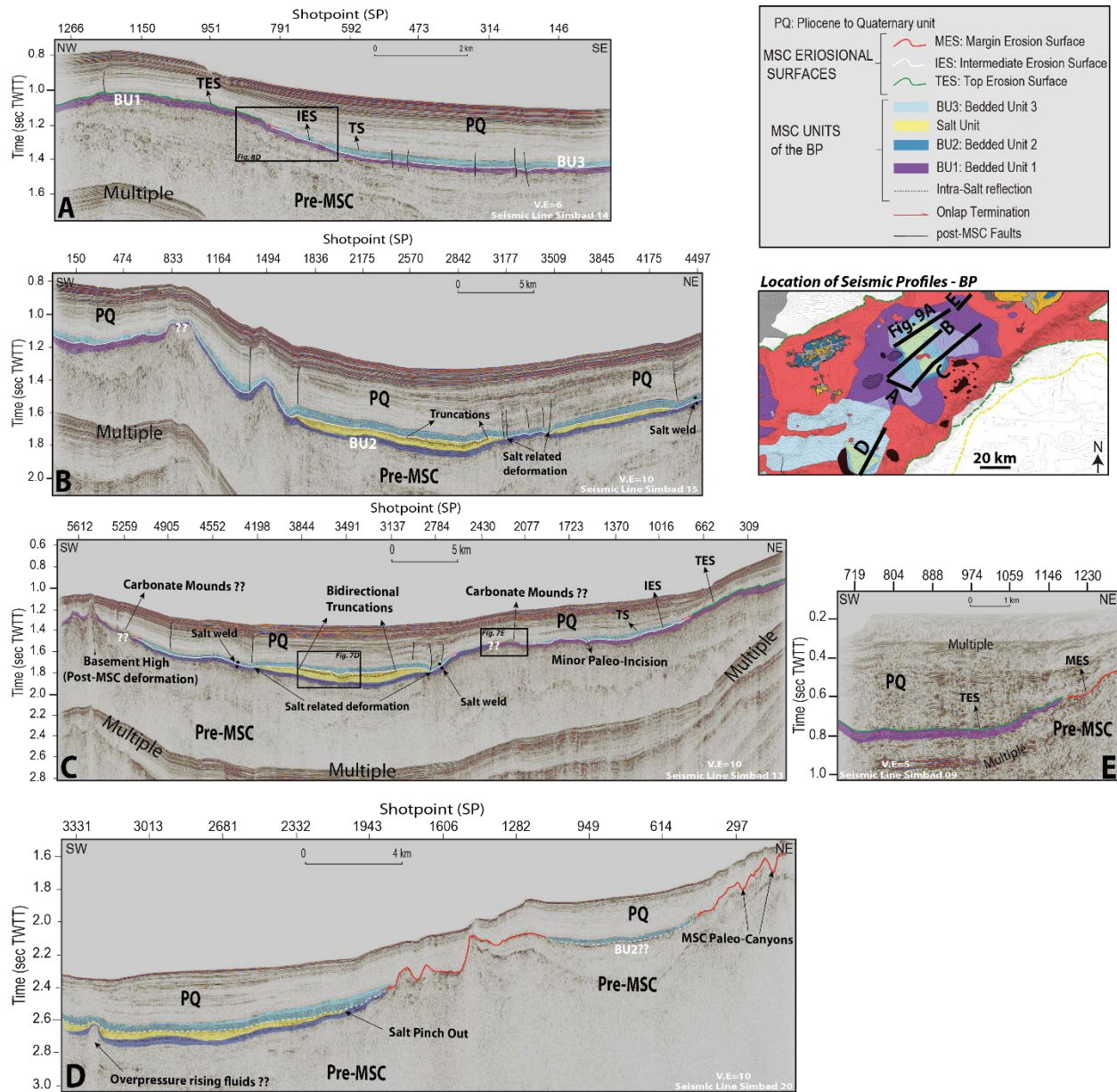
524

525 4 Results: MSC markers of the CMD/BP

526 Seismic units and their bounding surfaces are well expressed and preserved in the CMD (Figs.
527 5B and 5C). Four MSC seismic units and several conformable or unconformable bounding
528 surfaces were identified from high-resolution seismic profile's interpretation, based on their
529 seismic facies and on their geometrical and seismo-stratigraphic positions and relationships.
530 They are described hereafter.

531

532



533
 534 **Figure 5.** Seismic profiles covering different parts in the BP area. A: interpreted seismic profile Simbad 16 imaging
 535 the MSC seismic units in the southern part of the CMD, at the base of the Ibiza slope, where BU3 onlaps BU1. B-C:
 536 Interpreted seismic profiles Simbad 15 and Simbad 13 crossing the depocenter of the CMD showing all the MSC
 537 units and erosional surfaces. Note the bilateral truncation of the internal reflections intercalated in the salt unit
 538 due to an erosional event. D: Interpreted seismic profile in the southern depression of the Formentera Basin
 539 showing the presence of salt lying between 2 bedded units. E: Part of interpreted seismic profile Simbad 09
 540 showing the thinning of BU1 passing into a Marginal Erosional Surface (MES) on the present-day southern shelf of
 541 Mallorca.

542

543

544

545 - **Bedded unit 1 (BU1)**: this unit is widespread, mainly on the present-day shelves and slopes of
546 the BP, ranging from a minimum present-day depth of ~170m below sea level beneath the
547 shelves to a maximum of ~1200m beneath Mallorca slope (Figs. 3A and 5C, SP 2077). Its
548 extension has been underestimated in previous studies (Driussi et al., 2015; Ochoa et al., 2015),
549 as our new seismic dataset shows its wider presence on the Alicante shelf and on the shelf
550 between Menorca and Mallorca islands. On oil industry profiles, BU1 is contained in 1 or 2
551 reflections, whereas on high resolution seismic profiles, it is made of up to 8, medium to high-
552 amplitude, relatively low frequency, reflections (Fig. 6 D-F). In the proximal domain, BU1 is
553 overlain by the lower Pliocene unit and underlain by pre-MSC units (Fig. 5A, SP 791 to 1266; Fig.
554 5C, SP 1 to 662), respectively made of very low and low amplitude reflections. In more distal
555 domains, BU1 is overlain by another MSC unit (BU3, described later in this section) and still
556 underlain by pre-MSC sedimentary unit (Fig. 5A, SP 146 to 791; Fig. 5B, SP 150 to 833; Fig. 5C,
557 SP 1016 to 2077).

558 The upper boundary of BU1 is marked by a regional erosional surface (TES or IES) (Fig. 5A, SP
559 791 to 1266; Fig. 5C, SP 309 to 2077; Fig. 6 D-F) evidenced by truncated reflections (Fig. 6F).
560 This erosion locally draw ~10 to 30ms TWTT deep V to U-shaped incisions (Fig. 5C, SP ~1500).
561 The lower boundary of BU1 is generally concordant with the underlying pre-MSC units (BS),
562 except locally, where the unit is internally deformed with an apparently unconformable base,
563 probably due to seismic artefacts (Fig. 6E). Both the upper and the lower boundaries show an
564 abrupt amplitude change, evidencing high impedance contrasts between the BU1 and the
565 overlying Pliocene and underlying pre-MSC units (Figs. 5 A-C and 6 D-E).

566 BU1 is characterized by several internal seismic facies alternating high amplitude continuous
567 parallel reflections (bedded facies) (Fig. 6 D and F; Fig. 6E, SP 1376 to 1565) and medium
568 amplitude deformed reflections (chaotic facies), observed especially on the slopes (Fig. 6E; SP
569 1565 to 1908). Reflection free facies is also locally found.

570 The thickness of BU1 is relatively constant along the BP (Fig. 6 D-F), with an average thickness
571 of ~ 110m. It is thinner (~60m; Fig. 5E) near the coastline of Mallorca, between Palma and
572 Campos Basins, as a result of the partial erosion of the unit. Where not/slightly eroded or
573 deformed, BU1 reaches a thickness of up to ~130m on the slopes (Fig 6E, SP 1467). BU1 is

574 however, most of the times, absent on the shelves where only the MES is observed (Fig. 3A and
575 4A; Fig 5E, SP 1230). BU1 apparently thins out downslope (Fig. 5A, SP 592 to 1150), but its
576 lateral continuity is unclear (Fig. 7E). On the seismic profile Simbad 14 (Fig. 5A) however, it
577 seems continuous downslope.

578 - **Bedded unit 2 (BU2)**: on oil industry seismic profiles it appears as a single reflection. On high-
579 resolution profiles, it consists of up to 5 medium- to high-amplitude, relatively low frequency
580 reflections. BU2 is overlain by the salt unit (see description of this unit later in this section) in
581 the depocenters (Fig. 5B, SP 1836 to 4497; Fig 5C, SP 2784 to 4198; Fig. 5D, SP 1943 to 3331),
582 whereas on the slopes, where there's no salt, it is lying below another MSC unit, labelled BU3
583 (Fig. 5B, SP 833 to 1823; Fig. 5C, SP 4198 to 5259). BU2 is everywhere lying above pre-MSC
584 sediments (Fig. 5 B-D).

585 In relatively proximal zones, the upper boundary of BU2 appears to be an erosional surface with
586 some incisions (~5-10ms TWTT; Fig. 9, SP 991), whereas in the deeper depocenters it is
587 conformable with the overlying salt unit (Fig. 5B, SP 1836 to 2842). The lower boundary of BU2
588 is concordant with the pre-MSC units, but the low acoustic impedance contrast between those
589 units makes it difficult to firmly identify the base of BU2.

590 The internal reflection pattern of BU2 is characterized by parallel reflections laterally
591 continuous in the distal domain but their lateral continuity weakens moving towards the
592 proximal domain (Fig. 5C, SP 2430 to 5259).

593 The maximum observed thickness of BU2 is 50ms TWTT (~ 110m to 65m depending on its
594 internal lithology; see discussion for details). This thickness may be underestimated as the base
595 of BU2 is uncertain, especially in the deepest part of the CMD. The lateral extent of BU2 toward
596 shallower depths is also not clear and its relationship with the BU1 not properly imaged (Fig.
597 7E). It is not excluded that BU2 could be the distal continuation (and thus the time equivalent)
598 of BU1, accumulated in a more proximal domain (Figs. 5C and 9A), but additional profiles would
599 be needed to confirm this geometry.

600 Figure 5C (SPs 2077 to 2430; SP 5259) features an approximately 1.5km wide mounded
601 structure overlain by the lower Pliocene and apparently lying directly above BU1 (Fig. 7E). It is
602 observed on the borders of the depocenter, close to the pinch-out of BU3. The seismic

603 signal around this feature does not allow us to figure out if any of the BUs has onlap
604 termination on the structure. Onlap terminations and draping of the base reflections of the PQ
605 unit on this mounded feature can be observed.

606

607 - **Salt unit:** this unit displays a classical dominantly reflection free (transparent) facies (e.g. Lofi et
608 al., 2011a, b). Internal low-amplitude low-frequency continuous reflections are commonly
609 observed in this unit (Fig. 5B, SP 2570 to 3177; Fig. 5C, SP 3137 to 3844; Fig. 9A, SP 1274 to
610 2122). The salt unit lies everywhere below BU3 and above BU2 (Figs. 4 B and C; Fig. 5 B-E).
611 The upper boundary of the salt is an unconformable surface marked by a truncation of the
612 topmost internal reflections (Fig. 4 B and C; Fig. 9A). The base of the salt is clearly concordant
613 with BU2.

614 Its maximum thickness is ~240m, reached in the deepest part of the CMD.

615 The base of the salt (top BU2) remains locally uncertain because of the poor imaging below the
616 salt on high-resolution seismic data, but crossing with confidential re-processed oil industry
617 profiles confirmed its location at 1.8 - 1.9 sec TWTT in the CMD (Fig. 5 B and C) and not deeper
618 as questioned by Maillard et al. (2014). Toward the borders, the salt thins out as a wedge. Due
619 to the ductile deformation of the salt, its pinch-out termination is often associated with listric
620 faults and brittle deformation of the overlying BU3 and PQ units (Fig. 5B, SPs 1836, 3177 and
621 ~4250). These listric faults, together with the deformation of the units overlying the salt,
622 suggest that originally the salt extension was locally wider, and that it later glided towards the
623 depocenter, leading to formation of salt welds (Fig. 5C). Moreover, the current thinning of the
624 salt (wedge geometry) towards the borders of the salt basin is not an expression of progressive
625 onlap of younger layers. It results from an erosion evidenced by the truncation of the intra-salt
626 reflections, more and more into deeper (older) levels towards the margin.

627 Seismic profile Simbad 13 shows that the top of the salt exhibits locally a concave U-shaped
628 depression lying above down-warped internal seismic reflections (Fig. 5C, SP 3491). The relief
629 extends for about 1.5 km horizontally along the seismic profile. Down-warped reflections are
630 also observed in the BU3 and PQ deposits overlying the depression but the deformation is
631 progressively attenuated upwards (Fig. 7D).

632 - **Bedded unit 3 (BU3)**: on oil industry profiles it is made of 2 reflections, whereas on high
633 resolution profiles it consists of up to 9 low- to medium-amplitude, high frequency reflections
634 (Fig. 8F). BU3 is everywhere conformably overlain by the lower Pliocene. In proximal domains, it
635 unconformably overlies either the MES (Fig. 5D, SP 1943) or BU1 or BU2 (Fig. 5A, B). Internal
636 reflections of BU3 show onlap terminations on the erosion surface (IES) bounding above
637 BU1/BU2 (Fig. 8D, E). More distally, in the depocenters, BU3 conformably overlies the salt unit
638 (Figs. 5 A-D and 8 D, E). On the border of the salt basin, BU3 is often affected by brittle
639 deformation related to the ductile deformation of the underlying salt (Fig. 5C, SPs 2784 and
640 4198).

641 The spatial extent of BU3 is limited to some of the BP sub-basins (Fig. 3A). BU3 shows no lateral
642 continuity or geometrical connection with the UU accumulated in the deeper basins
643 surrounding the BP (Fig. 3A).

644 The internal facies of BU3 consists dominantly of parallel and clearly continuous reflections in
645 the distal part of the CMD and Formentera Basin (Figs. 5 A-D and 8F). It becomes hummocky
646 and relatively chaotic towards the proximal areas (Fig. 8E). In shallower sub-basins, such as El
647 Cid and Cogedor Basins, BU3 overlies BU1 and appears as a very thin unit, with less beddings
648 and irregular top (Fig 6D, SP 3848).

649 The thickness of BU3 is variable. In the CMD it reaches a maximum thickness of ~120m in the
650 structural lows and/or in flat regions at the foot of slopes (Fig. 8F). In the southwestern basins
651 of the BP, e.g. El Cid Basin, BU3 appears very thin on high-resolution seismic lines and thus
652 cannot be distinguished from BU1 on the low-resolution seismic lines. Consequently, its
653 presence might be underestimated in the south-western part of the BP, where we have scarce
654 high-resolution seismic coverage (Fig. 3).

655

656 The PQ unit overlies BU3 in the distal domain (Fig. 5B-D). In proximal domains it overlies BU1
657 where present (Fig. 5E, SP 719 to 1146) or the MES where BU1 is absent (Fig. 5D, SP 297; Fig.5E,
658 SP 1230). The basal part of the PQ unit is characterized everywhere on the BP by a very low
659 amplitude reflectivity (Figs. 5 and Fig. 6 D-F), except locally (e.g. Fig. 5B, SP 3845). The pattern
660 of the basal reflections of the PQ unit in the CMD shows a clear sheet-like shape, draping the

661 topography of the underlying Messinian units (Ludmann et al., 2012). On the Mallorca slope it is
662 deformed by the post-MSC gliding affecting BU1 (Fig. 6E; Maillard et al., 2014).

663

664

665 5 Interpretation/Discussion

666 5.1 Sicily vs Balearic Promontory: depositional units, surfaces and geometries

667 Several sedimentary models were proposed to account for the MSC deposits observed in the
668 Sicilian Basins (Fig. 4 E-G), starting from the oldest models by Decima and Wezel (1971) and
669 Garcia-Veigas et al. (1995), to more recent models by Rouchy and Caruso (2006) and Roveri et
670 al. (2008). In all these models the depocenter of Caltanissetta Basin contains a halite unit
671 sandwiched between two MSC units, the LE and the UE. Our seismic observations evidence that
672 the MSC units in the BP, especially in the CMD, show a similar configuration: in the depocenter
673 there is a salt unit (Fig. 4A) sandwiched between two other MSC units, BU2 below and BU3
674 above (Fig. 4 B, C).

675 The distribution of the MSC deposits in Sicily has been described schematically by Roveri et al.
676 (2006) (Fig. 3D). In their model, only the marginal sub-basins such as Calatafimi Basin contain in
677 situ PLG deposited in shallow context, whereas deeper basins such as Belice Basin contain only
678 RLG (see section 3). The even deeper sub-basins of Caltanissetta are the only basins where salt
679 and the upper evaporites are found (Figs. 3D and 4D). A very similar distribution is remarked in
680 the BP, where the shallow perched sub-basins usually contain exclusively BU1, locally topped by
681 a very thin BU3 with an irregular but non-erosional top (Fig. 6D). The deeper sub-basins
682 (Formentera Basin; Fig. 5D and CMD; Fig. 5B, C) contain BU2 and a thick BU3, together with the
683 salt unit in between (Fig. 3A).

684 Herein we discuss a possible analogy between Messinian Sicilian basins and BP sub-basins,
685 assuming that the MSC seismic units of the BP, described in the previous section, could be the
686 equivalent of the Sicilian MSC units described in section 2.2.

687 Observations of Messinian sub-basins from both BP and Sicily show a high analogy between the

688 evaporitic units in terms of geometry, facies and distribution. In our comparison we will focus
689 mainly on the CMD and CB.

690

691 5.1.1 Geometry Similarities:

692 a- In the north-eastern part of the CB, seismic profiles imaging MSC sediments in a
693 relatively undeformed or slightly deformed perched sub-basin (Fig. 9B, C), show that this
694 depression has a concave-like geometry. The MSC unit is thicker in the depression's
695 depocenter and includes salt, whereas towards the borders of the depressions, the salt
696 pinches-out and there is a notable thinning of the MSC units. This geometry is very
697 similar to the one observed in the CBD (Figs. 5C and 9A).

698

699 b- The top of the PLG in Sicily is cut by a regional erosional surface in the shallower parts of
700 the basins (Fig. 6A, C) and is locally overlain by the lower Pliocene Trubi Fm. Similarly, in
701 the proximal part and the slopes of the BP, the top of BU1 is cut by a regional erosional
702 surface (TES in Fig. 6E) and is overlain by the lowest Pliocene unit.

703

704 c- Towards the depocenter, in the CB, the UE overly the LE and the contact between those
705 2 units is often marked by an erosional surface (Fig. 8A, B; and Roveri et al., 2019). In the
706 distal areas of the BP, BU3 overlies BU1 and the contact between the two units is also
707 erosional (IES in Fig. 8D, E).

708

709

710 d- The MSC salt in the CB is lying between 2 units (i.e. LE and UE; Figs. 4 E-G and 7A) and is
711 found in the depocenters. Towards the margins, the salt unit pinches out where LE and
712 UE become in contact along an erosional surface.

713 Exactly the same configuration is observed in the CMD, where the MU is underlain by
714 BU2 and overlain by BU3 in the depocenter (Fig. 5B, C). Toward the margin of the

715 depression, the salt pinches out where BU2 and BU3 are in contact along an IES (Figs.
716 4B, C).

717
718 e- In the depocenters of CB, the UE lie on the salt, where the transition is defined by a
719 meter-thick laminar cumulate gypsum horizon (Fig. 4F). In a more proximal location, on
720 the borders of the basin, clear onlap terminations of the UE against the LE (PLG and/or
721 CdB) is observed (Fig. 8A, B; Decima and Wezel 1971; Rouchy and Caruso 2006; Roveri et
722 al., 2008).

723 A similar geometrical relationship exists in the CMD, where the post-salt BU3 lies above
724 the salt unit (Fig. 4B, C) in the depocenter and onlaps BU1/BU2 (Fig. 5B, SPs 309 to 2077,
725 and 4198 to 4905) in the proximal domains of the basin (Fig. 5A, SP 791; Fig. 5C, SPs
726 ~800 and ~5100; Fig. 8D, E).

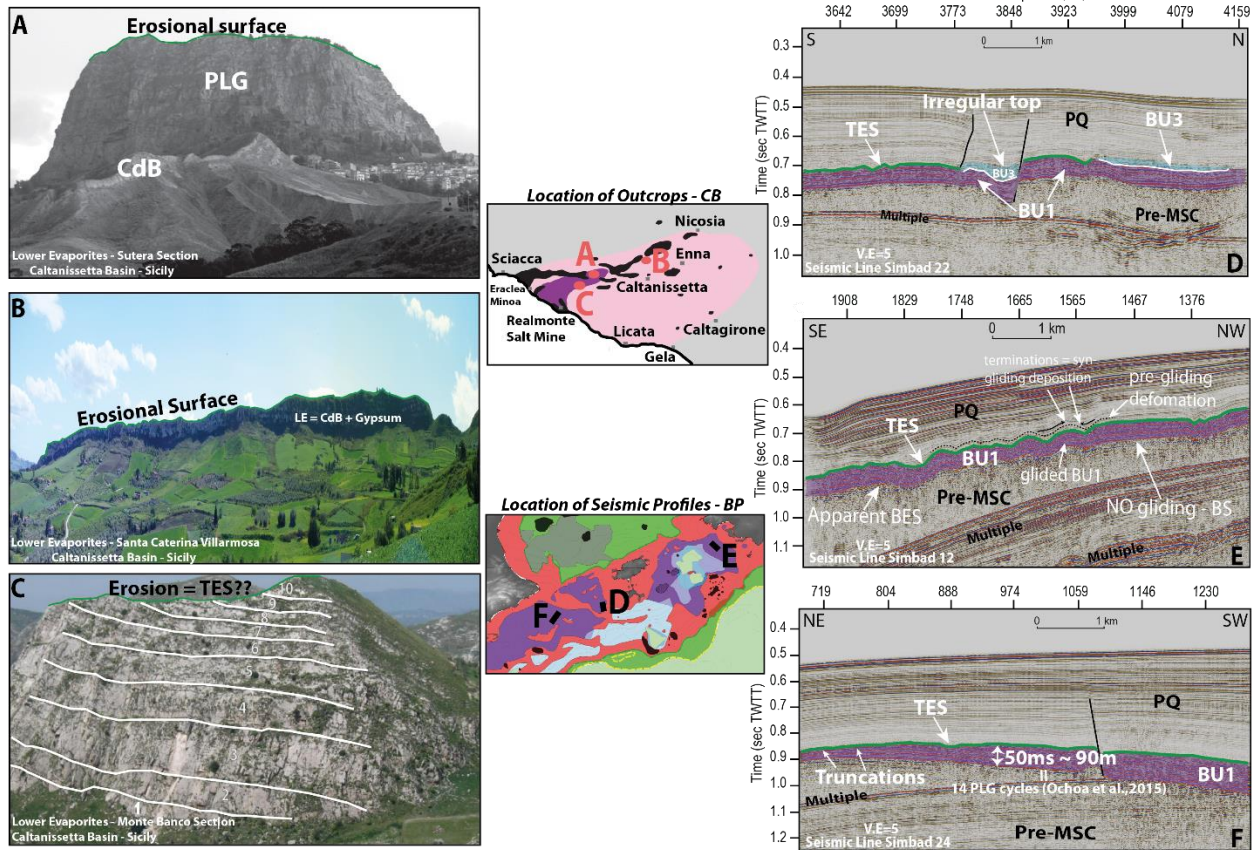
727

728 5.1.2 Facies Similarities:

729 a- **PLG vs BU1**

730 The PLG in the CB has been described and correlated across the Mediterranean by Lugli
731 et al. (2010). It consists of processional driven cycles of primary gypsum separated by
732 shale horizons. Ochoa et al. (2015) demonstrated that the BU1 of the Elche sub-basin
733 also corresponds to the PLG. It is made of cyclical gypsum/marl alternations (up to 14
734 cycles; Fig. 6F) and displays a bedded seismic facies (see section 4, BU1), as expected
735 from such internal lithologies. This bedded seismic facies is typical of the BU1 and is
736 observed at the scale of the promontory, suggesting that BU1 is the equivalent of the
737 PLG everywhere on the BP, and not only in the Elche Basin. The erosional surface at the
738 top of BU1 (Fig. 6 D-F) supports for its interpretation.

739



740

741 **Figure 6.** Figure illustrating the comparison between the Lower Evaporites (LE) and Bedded Unit 1 (BU1) in CB and
 742 BP, respectively, both belonging to stage 1 of the MSC. A: Lower evaporites section in Sutera (CB – Sicily) showing a
 743 Primary Lower Gypsum (PLG) eroded at the top by an erosional surface (TES?) (modified from Manzi et al., 2011).
 744 B: Section of Santa Caterina Villarmosa showing the LE unit, cut by an erosional surface. C: Monte Banco section
 745 made of up to 10 PLG cycles eroded at the top (modified from Bonanni D.M. 2018). See Fig. 4D for the legend of
 746 the outcrops' location map. D: Interpreted part of seismic profile Simbad 22 showing the bedded facies of BU1 on
 747 the southern slope of Ibiza, where it is truncated at the top by the TES. Here another MSC bedded unit (BU3)
 748 appears to lie locally above BU1. The irregular top of BU3 is probably due to syn-depositional faulting. E: Part of
 749 interpreted seismic profile Simbad 12 showing different facies of BU1: its facies appears perfectly bedded when
 750 undeformed, whereas its facies becomes more chaotic when deformed by gliding. Note that the gliding affecting
 751 the unit is post MSC, which means it could not be compared to the RLG. F: Part of seismic profile Simbad 24
 752 located on the Alicante Shelf of south-east Spain, showing BU1 abruptly truncated at the top and thinning due to
 753 erosion towards the NE. Note that the seismic facies and the thickness of BU1 is similar in all sub basins in the BP,
 754 suggesting that it is everywhere made of stage 1 PLG cycles truncated at the top. See Fig. 3A for the legend of the
 755 seismic profiles' location map.

756

757

758 **b- BU2 vs RLG**

759 The RLG in Sicily consist of resedimented gypsarenites, gypsum laminates, and PLG

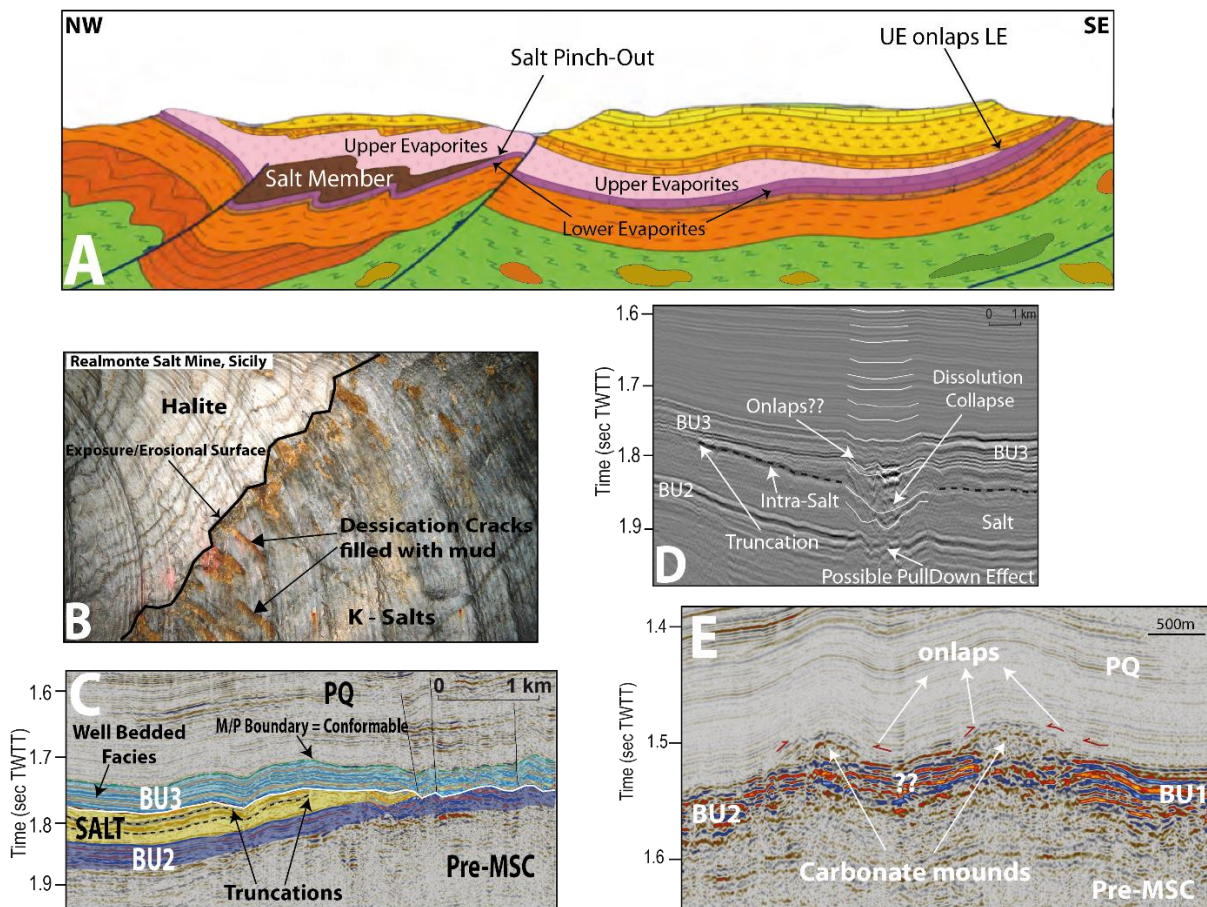
760 gypsum blocks. As already discussed in section 2.2, the origin of the large dislocated
761 blocks of RLG in the CB is controversial. However, both interpretations of RLG blocks
762 imply an active syn-tectonic activity in the basin for the block-sliding. This is not the case
763 in the BP, where the syn and post-tectonic movements are relatively negligible. In the
764 MSC records of the BP, we thus do not expect the presence of large olistostromes,
765 which could have been at the origin of internal chaotic seismic facies as stated by Roveri
766 et al. (2019). Thus, due to the geometrical position of BU2 below the salt, and the
767 relatively continuous reflections it contains, it could be the equivalent of the RLG of CB
768 made of gypsarenites and gypsum cumulates (sensu Rouchy and Caruso, 2006)
769 resedimented from BU1 as well as primary. However, in the CMD, the relationship
770 between BU1 and BU2 remains unclear. Both are clearly pre-dating the salt
771 emplacement, and BU2 seems at least partly lateral time equivalent of BU1, but with a
772 change in internal facies, that could be due to a change in the internal content in
773 gypsum (Fig. 5 B, C). At this stage, a firm link between BU2 and RLG is difficult to
774 establish.

775

776 c- **MU vs Halite**

777 The salt sequence in the CB consists mainly of Halite and K-Mg salts that show a clear
778 shallowing upward trend until reaching an exposure erosional surface expressed by
779 desiccation cracks (Fig. 7B; see section 3 and Lugli et al., 1999). In the CMD the salt
780 sequence is characterized by a globally transparent seismic facies with internal
781 reflections in its upper part (Fig. 4B, C; Fig. 7D). Those intra-salt reflections suggest that
782 it is not made of pure/unique salt. The uppermost reflection is truncated abruptly at the
783 top, which could be due to subaerial exposure or dissolution in shallow water. The
784 erosional surface observed in the Realmonte mine of the CB (Fig. 7B) is found inside the
785 salt unit and not at the top of it as in the salt observed in the CMD. The presence of a
786 major erosion on the top of the salts in CB could not be excluded, as also described in
787 the model of Decima and Wezel, 1973 (Fig. 4E). In fact, there could be several minor

788 erosional/exposure surfaces inside the salt unit of the CMD as well, with only the major
 789 one visible at a seismic scale.
 790



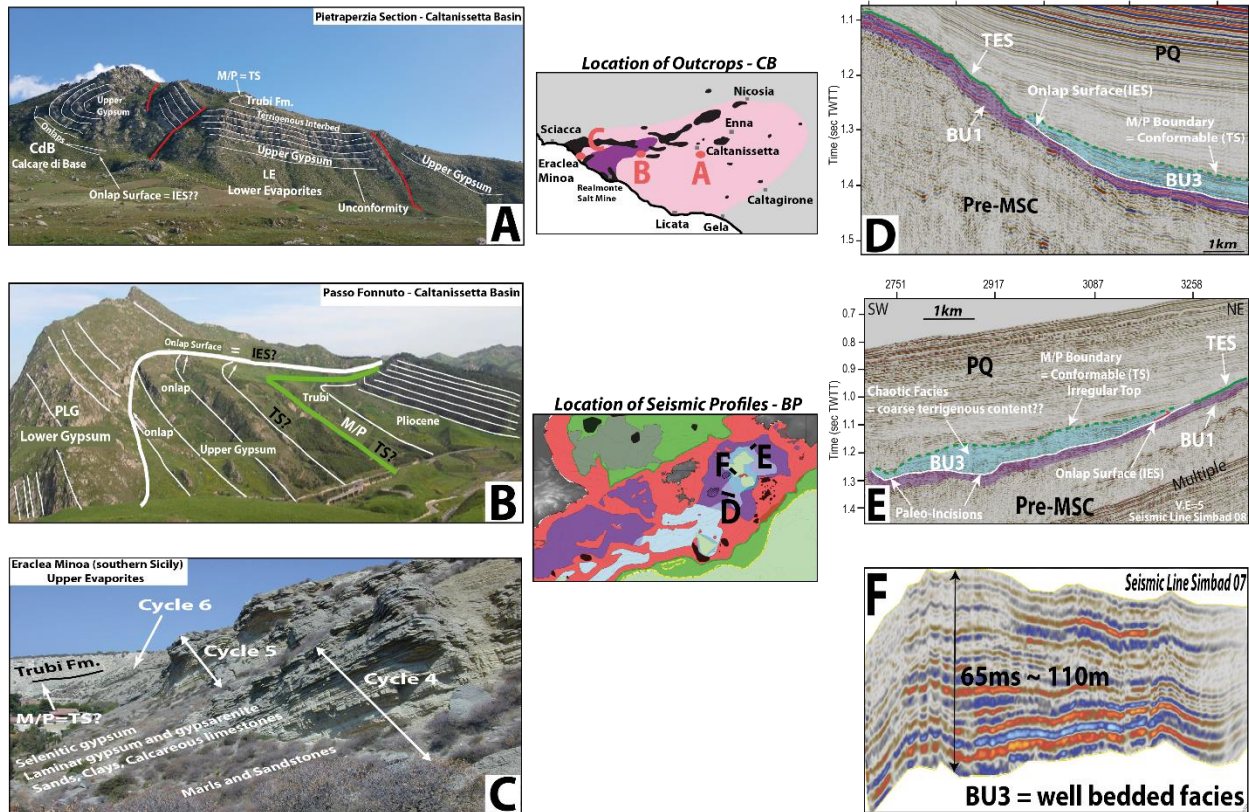
791
 792 **Figure 7.** Figure showing the geometrical settings and facies of the salt unit in CB and BP. A: Geological cross
 793 section between the towns of Caltanissetta and Enna in CB (position in Fig. 4D; modified from Carta Geologica
 794 Italiana, Caltanissetta, foglio 631). The section shows how the salt formation (here deformed by regional tectonics)
 795 belonging to the MSC is lying in between the lower and upper evaporites in the center of the section and it
 796 pinches-out in NW and SE directions, where the LE and UE become in contact. Note the onlap of the UE on the LE
 797 in the southeastern border of the basin. B: The MSC salt at the Realmonite Mine, CB, Sicily, showing an exposure
 798 surface at the top of the K-Mg salts with the desiccation cracks and the passage to halitic salts. C: Part of the
 799 seismic line Simbad 15 showing the truncation of the internal reflections at the top of the salt and illustrating an
 800 erosional surface which we interpret as an exposure surface or a dissolution surface in shallow water. Note how
 801 the salt unit in the BP, equivalent to CB's salt, is sandwiched between two other MSC units in the central basin:
 802 where the salt pinches-out, the underlying BU2 and overlying BU3 units become in contact. D: Zoom from seismic
 803 profile Simbad 13, showing a concave feature on the top of the salt, and associated down-wrapped reflections
 804 below and above, possibly related to salt dissolution at depth and associated cover collapse. E: Zoom showing the
 805 facies of the interpreted carbonate mounds (see text for details). It also shows the uncertainty about passage from
 806 BU1 to BU2.

807
808
809
810
811
812
813
814
815
816
817
818
819
820
821
822
823
824
825
826

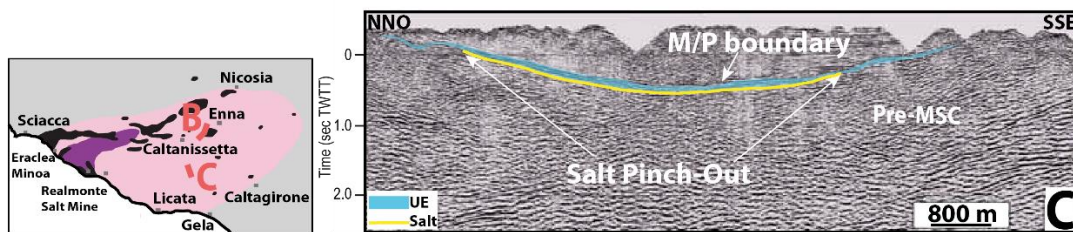
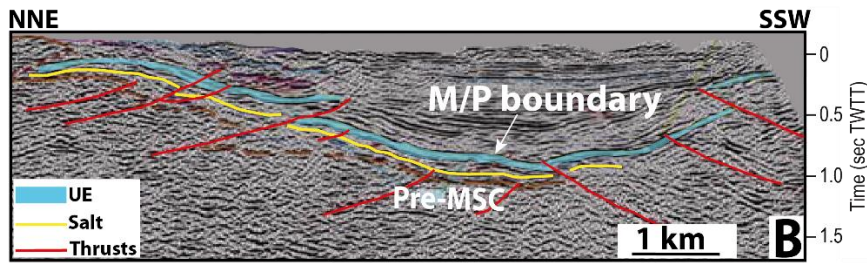
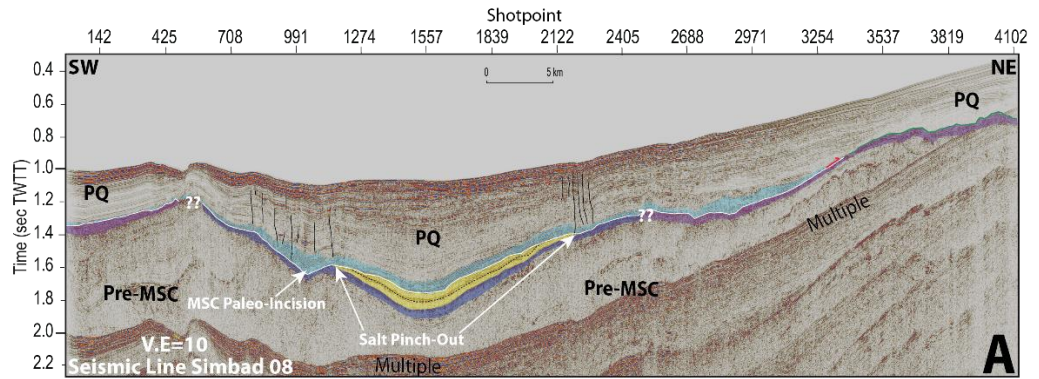
d- **UE vs BU3**

The thickness of the UE unit reaches its maximum in the depocenter of CB. Its sedimentary facies is characterized by thick mudstone, sandstone and marl intercalations (Fig. 8C; see section 2.2). Towards the margins of the basin this unit thins out until onlapping the LE, and the terrigenous layers tend to decrease and be rich in coarser material (Fig. 8A).

This is an adequation with the characteristics of BU3. This unit reaches its maximum thickness in the distal part of the perched basins, especially in Formentera Basin and the CMD (Fig. 8F) and thins out towards the proximal part of the basins (Fig. 8D, E), where it onlaps the underlying unit. Moreover, the seismic facies of BU3 changes laterally from the distal to the proximal domains, passing from a well bedded horizontal unit (Fig. 4B and Fig. 8F) into a more discontinuous, less bedded one (Fig. 8E). This facies change could be due to the finer granulometry of the clastic intercalations between gypsum beds in the depocenter (shales to sandstone?) and coarser grain in more proximal context (conglomerates?).



827
 828 **Figure 8.** Figure showing the similarities between UE and BU3 in CB and CMD, respectively. A: Pietraperzia section
 829 (central CB – Sicily); Deformed upper gypsum cycles with terrigenous content in the uppermost cycle, showing
 830 onlap termination on the CdB along an erosional surface IES. B: Passo Fonnuto section (CB – Sicily; modified from
 831 Roveri et al., 2019); UE onlapping LE along an erosional surface. Note that the lower Pliocene formation (Trubi) is
 832 conformable with the UE (TS?). C: The upper evaporites cycles of the Eraclea Minoa section (CB – southern Sicily);
 833 the cycles are made of selenitic and clastic gypsum intercalated with levels of marls, limestones and clays. This
 834 facies is considered to be the most complete and has been deposited in the depocenter of the CB. For the legend
 835 of the outcrops' location map see Fig. 4D. D: Zoom from seismic profile Simbad 14 showing the onlap of BU3 on
 836 BU1 along an erosional surface (IES) on the southern border of the CMD. Note the poor beddings of the horizons of
 837 the PQ unit and the continuous (conformable) transition from the MSC to PQ. E: Part of seismic line Simbad 08
 838 showing the onlap geometry of BU3 on BU1 on the northern border of the CMD along an erosional surface (IES).
 839 Note how the IES is characterized by Messinian paleo-incisions whereas the top of BU3 is conformable with the PQ
 840 unit. BU3's facies is poorly bedded here probably due to coarse terrigenous content, explaining its thickening. F:
 841 Figure showing the perfectly bedded facies of BU3 in the deep depocenter of CMD where it reaches its maximum
 842 thickness. It's worth noticing how both BU3 and UE change their facies from the depocenter into the borders of
 843 the basins and how both units onlap an older MSC unit along an erosional surface.
 844
 845



846
 847 **Figure 9.** Interpreted profiles from both BP and CB showing the similarity in the shape and geometry of the sub-
 848 basins, especially here where a post-MSD flexure affected locally the CMD. A: Seismic profile Simbad 08 crossing
 849 the CMD from the southern to the northern part through the depocenter (position and legend in Fig. 5). Note that
 850 the salt is exclusively found in the deepest part of the CMD, whereas to the borders it pinches-out. B: Onland
 851 seismic profile near Capodarso (CB – Sicily, modified from Catalano et al., 2013). C: Onland seismic profile in the
 852 central part of CB (modified from Catalano et al., 2013). See Fig. 4D for the legend of the location map. Note how
 853 in both the CMD and CB, the MSC sediments are contained in a concave-shaped depression with only the deepest
 854 part containing salt.

855

856

857 5.2 CMD stratigraphy and relative chronology

858 In the offshore domain of the BP, ODP and DSDP scientific drillings do not exist. Oil industry
 859 drillings exist only on the Alicante shelf, on the southwestern part of the BP. They only offer
 860 borehole logs and cuttings providing discontinuous lithological record of the MSC depositional
 861 unit (Ochoa et al., 2015; Ochoa et al., 2018). Thus, the seismic method and onshore-offshore
 862 correlation approach are the only possible way to understand the history of deposition of the

863 MSC deposits at a regional scale. Hereafter we discuss the significance and the chronology of
864 the MSC units in the BP focusing on the CMD area based on the new interpretation of the
865 seismic dataset. Most importantly, these units show similarity with the Sicilian CB (section 5.1).

866 **BU1:** based on the following observations, we interpret BU1 as corresponding to the Primary
867 Lower Gypsum (PLG) deposited during the first stage of the MSC:

868 1- the proximal part of BU1 lies on a depth similar to the one of the PLG drilled onland in the
869 Palma Basin (~120-200 m below sea level; Rosell et al., 1998; Garcia-Veigas et al., 2018). They
870 also show similar thicknesses (80-90m; Rosell et al., 1998);

871 2- the seismic facies of BU1 is everywhere similar (see section 4.1 and Fig. 6 D-F) to the BU
872 drilled on the Alicante shelf and interpreted as PLG (Ochoa et al., 2015), which suggests that the
873 petro-physical characteristics of the unit are similar;

874 3- along the BP, BU1 is truncated almost everywhere by a regional erosional surface at the top,
875 sometimes expressed by a valley-shaped incisions (Fig. 5C), suggesting a subaerial exposure of
876 the unit during the MSC base level fall. This erosion could thus be the analog of the one at the
877 top of the PLG in other peri-Mediterranean MSC basins (e.g. Sorbas and Appenines; Roveri et
878 al., 2019; Roveri et al., 2001). The erosional top of the BU1 becomes less important moving
879 distally, which could reflect a shorter exposure time for subaerial erosion in distal areas and
880 progressive transition to subaqueous erosion towards more distal areas;

881 4- BU1 shows a high positive contrast in seismic impedance with the overlying PQ unit,
882 suggesting BU1 is made of harder rocks than the marls above, in agreement with the presence
883 of gypsum layers. BU1 locally shows internal reflection free facies (e.g. Fig. 5E, SP 719 to 804)
884 possibly reflecting the presence of thick gypsum cycles such as cycles 3 to 5 that are, summed
885 together, up to 60m thick and that have been correlated on the Mediterranean scale (Lugli et
886 al., 2010). This has been also hypothesized by Roveri et al., (2019) based on synthetic seismic
887 models (see their figure 10).

888 5- BU1 is locally deformed, showing internal chaotic facies (Fig. 5C, SP 309), probably due to the
889 gliding of the entire unit (Fig. 6E, SP 1565 to 1908), at the gypsum/pre-MSC interface. Since the
890 deformation also affects the lowermost overlying Pliocene strata (Fig. 6E), the gliding occurred
891 after the MSC. It could have been triggered by several factors, among which the increase in

892 slope angle with time, as a result of margin subsidence, favoured by the rheological contrast
893 between the gypsum layers and underlying clastic sediments (probably marls). Gliding along
894 gypsum interfaces has also been described by Bourrillot et al. (2010) in the PLG of the Sorbas
895 Basin. Locally, the internal chaotic facies could also be due to the presence of gypsum
896 supercones similar to the one described in the PLG of Sorbas Basin (branching selenite facies,
897 sensu Lugli et al., 2010).

898 Roveri et al. (2019) stated that BU1 in the CMD (SU) may correspond to chaotic deposits
899 emplaced by gravity flows containing small to giant PLG gypsum blocks. We believe that their
900 hypothesis is not correct, since RLG is known to be deposited in the second stage of the MSC,
901 whereas the gliding affecting BU1 appears clearly to be post MSC (Fig. 6E). Moreover, the RLG is
902 thought to be transported from margins and re-deposited basinwards (Roveri et al., 2008)
903 which is not the case for BU1 which shows an in-situ (< 1km) gliding without transport and re-
904 sedimentation. Moreover, except very little in the Palma Bay, no gypsum exists all around the
905 CMD's margins, so there is no possible source that such RLG might derive from.

906

907 **BU2:** the relatively high amplitude of some internal reflections of BU2 (Fig. 5C, SP 4198 to 5259)
908 suggests that this unit contains gypsum. Since the geometrical and temporal relationship
909 between BU1 and BU2 is not clear, we consider hereafter two possible alternative
910 interpretations for BU2:

- 911 - BU1 passes laterally to BU2 in the distal domain with a change in facies, and thus BU2 is
912 the lateral and time equivalent of BU1, deposited in MSC stage 1. This is supported by
913 several observations: 1- Locally, where BU1 is absent, we find BU2 currently lying at a
914 depth that coincide with the depth of BU1; 2- No onlaps are observed between BU2 and
915 BU1 and BU2 is never observed overlying BU1. In such case, several interpretations for
916 BU2 are possible. It could be made of marls and thin carbonatic layers deposited in deep
917 water conditions (equivalent in time to PLG being deposited in the shallower domain) in
918 the distal parts of the basin, similar to the one locally described in the CB by Manzi et al.,
919 (2011). It could be also made of shales similar to the one described in other Messinian
920 evaporitic basins such as the Piedmont Basin by Dela Pierre et al., (2011). However, such

921 shales and/or marls have usually a very low sedimentation rate, especially in areas not
922 very active tectonically. Considering the thickness of BU2 (maximum 65m for such
923 lithologies), it is unlikely that they could have been deposited during stage 1 of MSC
924 (duration of 0.37Ma). More in accordance with the observed seismic facies, BU2 could
925 also be made of pelagic primary gypsum cumulates depositing on the deep sea-bottom
926 as a snow fall (Warren, 2016) or on the shallower slopes and then resedimented in
927 deeper areas (De Lange and Krijgsman, 2010). An alternation between gypsum
928 cumulates and shales/marls is however not excluded. The downslope thinning of BU1 is
929 compatible with what has been observed for the PLG in the Piedmont Basin by Dela
930 Pierre et al. (2011).

931
932 - BU1 does not pass laterally to BU2, and BU2 is postdating BU1. This implies that BU2 is
933 post-dating stage 1 of the crisis, emplaced probably in stage 2. The lateral discontinuity
934 of the reflections of BU2 is the only observation that makes us doubt its continuity with
935 BU1 (Fig. 5B, SP 833 and 5C, SPs 2430 and 5259). In this case, BU2 could be the product
936 of erosion and re-sedimentation of BU1, possibly mixed with primary gypsum, as for the
937 RLG in the CB (Roveri et al., 2008). In such a case, the absence of chaotic facies and
938 diffractions in BU2 would imply that this type of RLG is likely made of gyps-turbidites
939 rather than dislocated PLG blocks.

940 We, moreover, interpret the mounded features described in section (4.1.1, BU2; Fig. 5C) as
941 microbial carbonate mounds. These carbonates could have been formed at the paleo-shoreline
942 during the maximum retreat of the sea-level in the acme of the MSC (during deposition of
943 BU3?), and they could be the equivalent of CdB or CdB1 described by Caruso et al. (2015) and
944 Manzi et al. (2011), respectively. Similar isolated carbonate buildups with identical seismic
945 facies has also been identified and described elsewhere in non-MSC contest (e.g. offshore
946 Ireland by Hovland (2008), their figure 5.3; offshore Philippines by Burgess et al. (2013), their
947 figures 6B and 8C; and offshore Indonesia by Ruf et al. (2012), their figure 7).

948

949 **Salt:** the salt unit fills the deepest parts of the CMD where it reaches its maximum thickness
950 (~240m). Salt tectonics is clearly observed (Figs. 4 B, C; Fig. 9A). The MU post-dates BU1 and
951 BU2 since it is lying above the latter and pinches out laterally on it, which proves that it was
952 deposited in a later stage of the MSC.

953 We propose that the salt unit is likely mainly made of halite like the other MSC salt bodies in
954 the Mediterranean (e.g. CB, Lugli et al., 1999; Levant Basin, Feng et al., 2016). The continuous
955 reflections in this unit might reflect a change in lithology from halite to Mg- and K-salts, as
956 observed in the Sicilian salt (Decima and Wezel, 1971) of the CB. This would indicate increased
957 brine concentration toward the top of the unit and could be related to a shallowing upward
958 depositional environment (Lugli et al., 1999).

959 Clastic intercalations have also been encountered in the MSC halite (MU) of the Levant Basin in
960 the eastern Mediterranean. The intercalations consist of layers of claystones (Gvirtzman et al.,
961 2013; Feng et al., 2016) and/or argillaceous diatomites (Meilijson et al., 2019). Such
962 intercalations give birth to high-amplitude high-frequency reflections on the seismic profiles
963 (Feng et al., 2016, their figure 2), due to the important change in the petrophysical
964 characteristics between halite and clay/diatomites. In the CMD, the internal reflections in the
965 salt unit are characterized by low-amplitude and low-frequency. This suggest only a slight
966 change in the petrophysical characteristics of the material at the origin of the reflection and we
967 thus believe that the reflections within the salt of the CMD are due to change of evaporite type
968 rather than to the presence of clastics.

969 The top of the salt in the CMD is marked by the truncation of intra-salt reflections (Fig. 7 B, C).
970 This erosional unconformity could be originated either by salt dissolution in under-saturated
971 shallow diluted water (Kirkham et al., 2020) or by subaerial exposure (Ryan, 1978), both
972 processes requiring a significant base level drop. Toward the borders of the salt basin, the fact
973 that the truncation cuts into progressively older stratigraphic levels in the landward direction
974 suggests that the salt was initially extending further landward and has subsequently been
975 removed from shallower depths, supporting the hypothesis of an important drop in the base
976 level associated with this erosional event. A similar geometry has been evidenced on in the
977 deep Levant basin where intra-salt truncations are interpreted as of subaerial origin (Ryan,

978 1978), in agreement with the presence further north of fluvial deposits deposited at the top of
979 the salt (Madof et al., 2019). In the CMD, we interpret the down-warped seismic reflections in
980 the salt and overlying units as possibly imaging a solution-subsidence structure (Fig. 7D) related
981 to the dissolution of the subjacent salt. Overburden collapse structures related to dissolution of
982 subjacent evaporites have also been evidenced in the Levant Basin by Bertoni and Cartwright
983 (2005) and Hubscher et al. (2009). We tentatively suggest that in the CMD, such a dissolution
984 may have been initiated during the lowstand phase contemporaneous with the erosion of the
985 top of the salt.

986

987

988

989 **BU3:** We interpret this unit as the possible equivalent of the stage 3 MSC deposits of the CB
990 (upper evaporites and the Lago Mare sub-stages). In the CMD, the important acoustic
991 impedance contrast between BU3 and the overlying lower PQ unit (probably marls and
992 calcisiltites similar to the lower Pliocene unit of Palma Basin; Capo and Garcia 2019) reflects an
993 important change in lithology. The internal stacking bedded facies of BU3 in the depocenter of
994 the CMD (Fig. 8F) is coherent with an internal lithology consisting of alternations of gypsum and
995 fine clastic sediments similar to the one described at Eraclea Minoa in CB. The low frequency
996 characterizing the facies of BU3 (Fig. 8F) with respect to the high frequency ones encountered
997 in BU1 could reflect the thicker layers of clastics included in it, similar to the clays and marls of
998 the UE (Fig. 8C). If present, the Lago Mare phase representing the end of the MSC could be
999 contained in the uppermost reflection of BU3 or included in the lowermost PQ horizon due to
1000 its reduced thickness.

1001 The aggrading pattern of BU3 suggests that, following the erosion of the top salt layer under
1002 lowered base-level, BU3 deposited in a topographic low forming a perched lake system. The
1003 onlap of the internal reflection of BU3 on the margin may reflect a rise in base-level, as the
1004 sediments infill the lake and the mean shoreline of the perched basin shoals through
1005 aggradation. This is in accordance with what proposed for the UE of the CB by Butler et al.

1006 (1995).
1007 Similarly to the centi-metric to deci-metric scale erosions described in the UE in CB due to the
1008 precession driven sea-level oscillations (Rouchy and Caruso, 2006), internal erosions within BU3
1009 might exist, but they are not visible at the seismic scale. The top of BU3 marking the Miocene-
1010 Pliocene (M/P) boundary is conformable in the CMD with no evidence of erosion on the seismic
1011 scale (Fig. 4B, C) suggesting that the perched lake always remained under water. The M/P
1012 boundary in CB is however interpreted as unconformable (see section 2.2, Arenazzolo member;
1013 Cita and Colombo, 1979). In other shallower sub-basins in the BP, a very thin BU3 appears
1014 locally. The irregular top could be due to mild syn-tectonic faulting affecting the unit (Fig. 6D).

1015 5.3 Proposed depositional scenario in the CMD and associated regional consequences

1016 Maillard et al. (2014) proposed several possible correlations between the different MSC
1017 markers of the BP, extending from onshore to offshore. Roveri et al. (2019) subsequently
1018 adapted one of the proposed scenarios (see their figure 14) to fit their 3-stages model.
1019 However, two crucial features were not considered in both previous works: the BU2 lying below
1020 the salt and the clear erosional surface truncating the top of salt.

1021 The approach that we use in this work and the similarities that we discussed between the CMD
1022 and CB, help us not only to constrain our understanding of the MSC in the BP, but also it could
1023 be a reciprocal way to answer some uncertainties about the MSC in CB.

1024 Thus, hereafter we propose a new scenario (Fig. 10) for the MSC in the CMD following our
1025 observations, interpretation, and comparisons and adapting the CIESM (2008) time
1026 chronological model for the MSC:

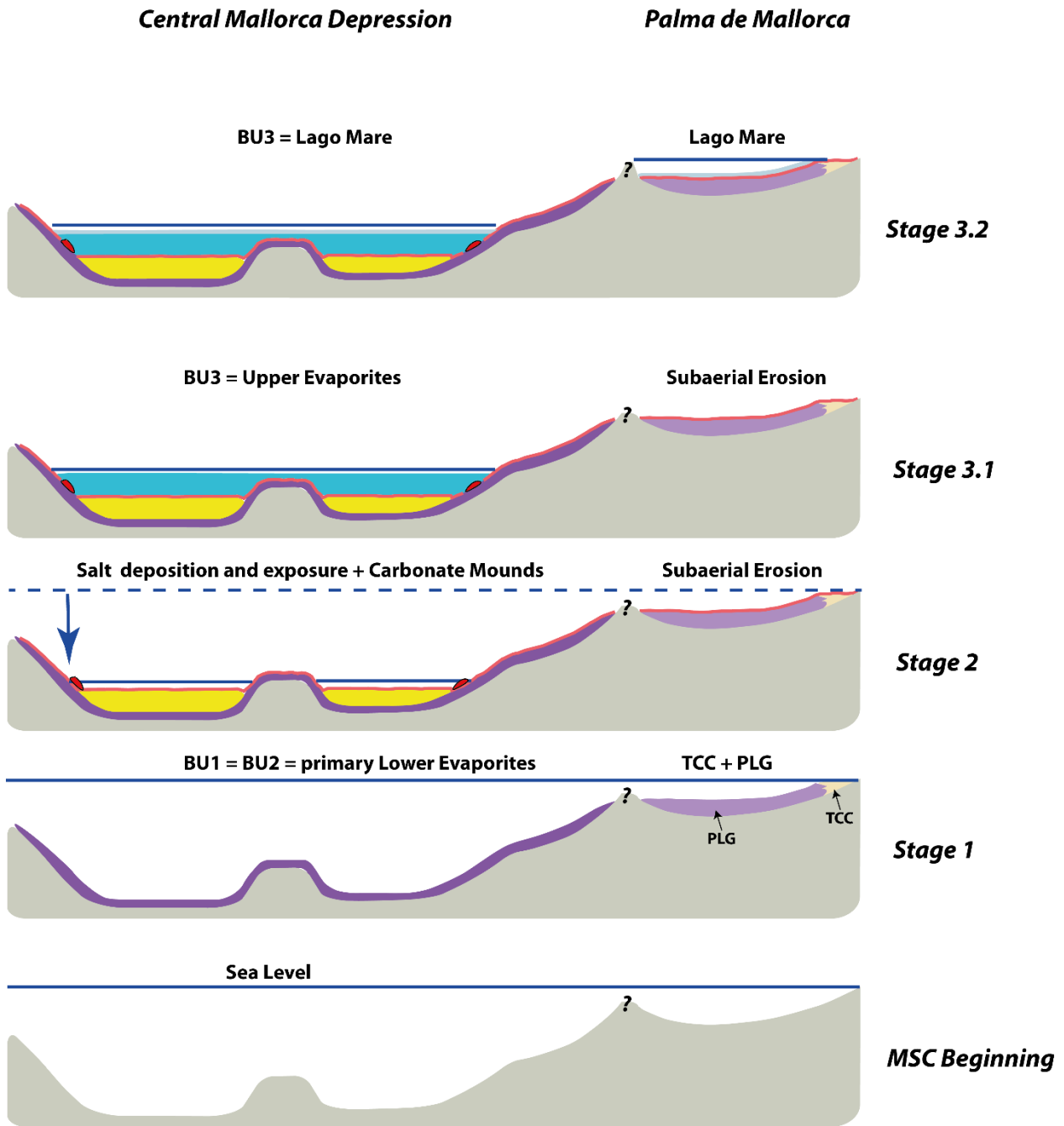
- 1027 - MSC stage 1 (5.97-5.60 Ma): during this stage, the Terminal Carbonate Complex (TCC), known
1028 also as Santanyi Limestones formation, has been deposited on Mallorca carbonate shelves
1029 contemporaneously with the Primary lower gypsum (PLG) in the Palma de Mallorca Basin (Mas
1030 and Fornos, 2012). Concurrently in the CMD, BU1 and BU2, which we interpret respectively as
1031 PLG and primary gypsum cumulates/marls, were deposited in continuity with the PLG of the
1032 southern Spanish basins, as equivalent to the lower evaporites unit of the Sicilian MSC basins.
- 1033 - MSC stage 2 (5.60-5.55 Ma): in this stage, a major base-level drop took place. The TCC and PLG

1034 already deposited in the proximal parts were undergoing an important subaerial erosion. In the
1035 depocenter of the CMD, salt bodies deposited in the 2 disconnected depressions, probably
1036 from high-concentrated salt brines. At the acme of this stage, the base-level dropped until the
1037 exposure and erosion of the top of the salt layers, marked by the truncation of the salt's
1038 internal reflections. This erosion could also be due to dissolution of salt in shallow waters. The
1039 salt's internal reflections likely reflect the change in the salt facies from halitic to kainite salts.
1040 At the border of the depression, microbial carbonate mounds deposited near to the paleo-
1041 shoreline. This carbonate formation might have continued also in the next stage. Moreover, the
1042 bidirectional truncation of the intra-salt reflections suggests that salt may have been eroded on
1043 the higher flanks of the basin during the acme of the crisis, and then re-deposited in the
1044 deepest part of the depocenter. This observation is evidenced by the presence of a pure salt
1045 transparent facies above the intra-salt reflections in the depocenter. This process might have
1046 acted also in the salts of CB, where above the desiccation cracks at the top of the K and Mg-
1047 salts lies a pure halitic unit that could have deposited due to the washing of salts deposited
1048 initially at the flanks of the depression and re-deposition in the deepest area, as also indicated
1049 by the Strontium isotopes values in this unit (Garcia-Veigas et al., 2018).

1050 - MSC stage 3 (5.65 to 5.33): during this stage, BU3 was deposited in the CMD. The bedded
1051 pattern of BU3 and its seismo-stratigraphic position suggest that it is likely affected by cyclicity
1052 similar to the one observed in the UE of the CB. The Lago Mare deposits were deposited in the
1053 CMD, as well as in the Palma Basin at the very end of this stage. This could have happened
1054 perched brackish lakes lying at different levels and that has received high volumes of fresh
1055 water from increased water runoff, similar to what observed in the Arenazzolo member in CB
1056 by Cita and Colombo (1979).

1057 Onland Mallorca, as well as at Eraclea Minoa in CB, the M/P boundary is marked by an
1058 unconformity reflecting the return of normal marine conditions following the Zanclean re-
1059 flooding. This unconformity is not observed on the seismic scale in the CMD. The lowermost
1060 horizons of the PQ unit in the CMD drapes the slopes up to the shelves, which indicate
1061 deposition in normal marine conditions (Fig. 5C; Ludmann et al., 2012).

1062



1063

1064 **Figure 10.** Proposed scenario of the MSC event in the CMD inspired from our new dataset interpretation and
 1065 comparison with CB, adapting the consensus age model of the CIESM (2008). Stage 1: deposition of BU1 and BU2
 1066 contemporaneously with TCC and PLG in the Palma Basin. Stage 2: Major sea-level drawdown during which the
 1067 units deposited in stage one, were exposed to intense subaerial erosion and the deposited in the depocenter from
 1068 two high-concentrated salt brines. At the paleo-shoreline, mounded carbonates equivalent to the CdB1 in CB
 1069 probably formed in this stage. Stage 3.1: Deposition of BU3 in the CMD, the equivalent of the Upper Gypsum of the
 1070 CB. Stage 3.2: Deposition of Lago Mare sediments from brackish-water lakes formed at different heights, probably
 1071 due to increased rivers run-off.
 1072

1073 6 Conclusions

1074

1075 The interpretation of a wide seismic reflection dataset covering the Balearic Promontory area
1076 allowed us to refine the mapping of the MSC unit's distribution and establish better the
1077 connection between the MSC sub-basins of the promontory. We were able to distinguish 4
1078 different seismic units based on their seismic facies and on their geometrical and stratigraphic
1079 relationships. Those seismic units are, from the oldest to the most recent one: BU1/BU2, Salt
1080 Unit and BU3. They are very well defined in the Central Mallorca Depression, where we have
1081 the best coverage among the basins in terms of density of high-resolution seismic data. The
1082 settings and geometrical relationships of the MSC units in the CMD show a strong analogy with
1083 the MSC sediments of the Caltanissetta Basin in Sicily, in terms of stratigraphic geometries,
1084 distribution and facies. In both the BP and Sicily, the Messinian deposits are situated in a series
1085 of sub-basins that were lying during the late Messinian at different water depths. The deepest
1086 basins accumulated a relatively thin (~300-500m) salt unit, sandwiched between two other MSC
1087 units. The comparison of the MSC units in the BP with the ones outcropping in Sicily allowed to
1088 constrain and propose a new 3-stages scenario for the MSC in the CMD.

- 1089 - The BU1 deposited first and is interpreted as equivalent to the bottom growth selenitic
1090 PLG found in CB and correlated on the Mediterranean scale (Lugli et al., 2010). BU1 is
1091 widespread and its present-day depth below sea level ranges from ~170m beneath the
1092 shelves to ~1200m beneath the Mallorca slope. The erosion surface at the top of BU1,
1093 restricted to the borders of the basins, is interpreted as of subaerial origin, when the
1094 base level of the Mediterranean was lowered.
- 1095 - The unit BU2, lying below the salt unit, is here considered as the temporal lateral
1096 equivalent of BU1 made of primary gypsum cumulates (snowfall) possibly mixed with
1097 clastic sediments.
- 1098 - Following the deposition of BU1/BU2, the salt unit filling the depocenters of the CMD
1099 accumulated in topographic lows forming perched sub-basins. It likely started depositing
1100 in relatively deep water and ended in shallow water. This unit is interpreted as halite
1101 rich where displaying transparent seismic facies, while the internal reflections may

1102 reflect K and Mg- salts. Their truncation strongly suggests a phase of subaerial exposure
1103 or dissolution under shallow water-column, contemporaneous with the Mediterranean
1104 base level lowering during the second phase of the crisis. The geometry of the intra-salt
1105 reflection truncations suggests that the salt layer in its entirety may have deposited
1106 higher up on the margin slopes before removal by erosion/dissolution.

1107 - Above the salt, the youngest MSC unit, BU3, is considered as the equivalent of the
1108 Sicilian Upper Evaporites, including the Lago Mare event. This last deposited in perched
1109 lakes fed with fresh waters and topographically disconnected from the surrounding
1110 deeper basins in which the base level was lower.

1111

1112 This work suggests that the CMD can be considered as an undeformed analog of the Sicilian CB.
1113 During the MSC drawdown phase, temporary perched lakes developed in sub-basins forming
1114 topographic depressions lying at intermediate water depths. During the acme of the crisis, the
1115 sea-level drawdown was thus important enough to disconnect the BP sub-basins from the
1116 Valencia Basin and the rest of the Mediterranean.

1117 The Sicilian MSC records (salt and the evaporites lying below and above it), classically provide
1118 key chronostratigraphic constrains for the MSC scenarios. They are often considered as
1119 representative of the deep basin records in particular to date the onset of the salt deposition at
1120 the Mediterranean scale. In our study, the clear absence of geometrical connection between
1121 the thin salt bodies found in the BP sub-basins and the thick salt layer from the deep Liguro-
1122 Provençal and Algerian Basins, however, indicate that salt deposition in perched basins is thus
1123 not necessarily contemporaneous with the deep basin salt, as also suggested recently by
1124 Meilijson et al. (2019) based on Eastern Mediterranean deep basin drillings. For the same
1125 reason, we also question the age and the origin of the thick, so-called, Lower Unit (LU),
1126 considered sometimes to be the equivalent of the outcropping Lower Evaporites. The CB salt
1127 and more generally its MSC records, should thus be used with care when trying to extrapolate
1128 the chrono-stratigraphy to the deep basin records.

1129 The change in facies between BU1 and BU2 described in this work and interpreted respectively
1130 as the passage at a certain depth range from primary bottom growth selenitic PLG to primary

1131 pelagic snowfall gypsum cumulates, is of an important significance as it might represent the
1132 maximum depth of formation of bottom growth selenitic gypsum in a non silled basin. In the
1133 BP, this depth is clearly exceeding the 200m threshold proposed by Lugli et al. (2010) and is in
1134 agreement with the work of Ochoa et al. (2015), thus suggesting that PLG is not strictly related
1135 to shallow perched basins.

1136

1137 **Acknowledgments:**

1138 This research is carried out under the SALTGIANT ETN, a European project funded by the
1139 European Union's Horizon 2020 research and innovation program under the Marie Skłodowska-
1140 Curie grant agreement number 765256.

1141 SALTGIANT ESRs and PIs are all thanked for the numerous exchanged discussions and
1142 comments during workshops, courses and fieldtrips. We are grateful to Francesco Dela Pierre
1143 for inspiring discussions on the Messinian Salinity Crisis. William B.F. Ryan is warmly thanked for
1144 the extremely constructive review and comments that significantly improved this manuscript.
1145 We also acknowledge the anonymous reviewer and the editor for their helpful comments.
1146 Spectrum and Western Geco Companies are thanked for providing seismic data that helped in
1147 the interpretation and mapping.

1148

1149

1150

1151

1152

1153

1154

1155

	Term	Acronym	Reference
	Messinian Salinity Crisis	MSC	
	Balearic Promontory	BP	
	Central Mallorca Depression	CMD	
	Caltanissetta Basin	CB	
	Bedded Unit	BU	
	Lower Unit	LU	
Offshore MSC units	Mobile Unit	MU	Lofi et al. (2011a, b)
	Upper Unit	UU	
	Complex Unit	CU	
	Lower Evaporites	LE	Decima and Wezel (1973)
	Upper Evaporites	UE	
Onshore MSC units	Primary Lower Gypsum	PLG	Roveri et al. (2006)
	Resedimented Lower Gypsum	RLG	
	Calcare di Base	CdB	Ogniben (1957)
	Terminal Carbonate Complex	TCC	Esteban (1979)
	Margin Erosional Surface	MES	

Onshore/Offshore MSC surfaces	Bottom Erosional Surface / Bottom Surface	BES / BS	Lofi et al. (2011a, b)
	Intermediate Erosional Surface / Intermediate Surface	IES / IS	
	Top Erosional Surface / Top Surface	TES / TS	

1157 **Table of acronyms.** Acronyms used in this paper for the study area and the MSC units, with the references to the
1158 origin of each term, where applicable.

1159
1160
1161
1162
1163
1164

Lofi et al. (2011a, b)	Maillard et al. (2014)	Driussi et al. (2015)	Ochoa et al. (2015)	Roveri et al. (2019)	This study
BU	BU	Ft	BU	BU - RLG	BU3
	Salt	Salt	Salt	Salt	Salt
	SU	MSC unit	BU - PLG	BU - PLG	BU2
					BU1

1165 **Table 1.** Synthesis of the Messinian units in the Balearic Promontory from all the offshore studies dedicated to the
1166 MSC.

1167
1168
1169
1170

1171
1172
1173
1174
1175
1176
1177
1178
1179
1180
1181
1182
1183
1184
1185
1186
1187
1188
1189
1190
1191
1192
1193
1194
1195
1196
1197
1198
1199
1200

References:

- Acosta, J., Canals, M., Lopez-Martinez, J., Munoz, A., Herranz, P., Urgeles, R., Palomo, C., Casamor, J.L. (2002). The Balearic Promontory geomorphology (western Mediterranean): morphostructure and active processes. *Geomorphology* 49, 177–204.
- Albanese, C., & Sulli, A. (2012). Backthrusts and passive roof duplexes in fold-and-thrust belts: the case of Central-Western Sicily based on seismic reflection data. *Tectonophysics*, 514, 180-198.
- Bache, F., Popescu, S. M., Rabineau, M., Gorini, C., Suc, J. P., Clauzon, G., ... & Londeix, L. (2012). A two-step process for the reflooding of the Mediterranean after the Messinian Salinity Crisis. *Basin Research*, 24(2), 125-153.
- Baron, A., Gonzalez, C. (1985). Correlation and geometry of the Messinian facies on the oriental edge of the Palma plain (Island of Mallorca). *6th European Regional Meeting Lleida* (5 pp., April).
- Bertoni, C., & Cartwright, J. A. (2006). Controls on the basinwide architecture of late Miocene (Messinian) evaporites on the Levant margin (Eastern Mediterranean). *Sedimentary Geology*, 188, 93-114.
- Bertoni, C., and J. A. Cartwright. (2005). 3D seismic analysis of circular evaporite dissolution structures, Eastern Mediterranean. *Journal of the Geological Society* 162.6: 909-926.
- Bonaduce, G. & Sgarrella, F. (1999). Paleocological interpretation of the latest Messinian sediments from southern Sicily (Italy). *Memorie della Società Geologica Italiana*, 54, 83-91.

- 1201 - Bonanni, D. M. (2018). The Messinian Salinity Crisis. The Mystery of the Vanished Sea. Volume 2.
1202 <https://en.calameo.com/read/0051898537b317dcb2d2c>
- 1203 - Bouillin J.-P., Durand-Delga M. & Olivier P. (1986) - Betic-Rifian and Tyrrhenian Arcs: distinctive
1204 features, genesis and development stages. In: Wezel F.C. (Ed.). *The Origin of Arcs, Elsevier*, 281-
1205 304.
- 1206 - Bourillot, R., Vennin, E., Rouchy, J.M., Blanc-Valleron, M.M., Caruso, A., Durllet, C. (2010). The
1207 end of the Messinian Crisis in the western Mediterranean: insights from the carbonate
1208 platforms of south-eastern Spain. *Sedimentary Geology* 229, 224–253.
- 1209 - Burgess, P. M., Winefield, P., Minzoni, M., & Elders, C. (2013). Methods for identification of
1210 isolated carbonate buildups from seismic reflection data. *AAPG bulletin*, 97(7), 1071-1098.
- 1211 - Butler, R. W. H., & Lickorish, W. H. (1997). Using high-resolution stratigraphy to date fold and
1212 thrust activity: examples from the Neogene of south-central Sicily. *Journal of the Geological*
1213 *Society*, 154(4), 633-643.
- 1214 - Butler, R. W., Lickorish, W. H., Grasso, M., Pedley, H. M., & Ramberti, L. (1995). Tectonics and
1215 sequence stratigraphy in Messinian basins, Sicily: constraints on the initiation and termination of
1216 the Mediterranean salinity crisis. *Geological Society of America Bulletin*, 107(4), 425-439.
- 1217 - Butler, R.W.H., McClelland, E., Jones, R.E. (1999). Calibrating the duration and timing of the
1218 Messinian salinity crisis in the Mediterranean: linked tectono-climatic signals in thrust-top basins
1219 of Sicily. *J. Geol. Soc. Lond.* 156, 827–835.
- 1220 - Camerlenghi, A., Accettella, D., Costa, S., Lastras, G., Acosta, J., Canals, M., & Wardell, N. (2009).
1221 Morphogenesis of the SW Balearic continental slope and adjacent abyssal plain, Western
1222 Mediterranean Sea. *International Journal of Earth Sciences*, 98(4), 735.
- 1223 - Camerlenghi, A., Del Ben, A., Hübscher, C., Forlin, E., Geletti, R., Brancatelli, G., ... & Facchin, L.
1224 (2020). Seismic markers of the Messinian salinity crisis in the deep Ionian Basin. *Basin Research*,
1225 32(4), 716-738.
- 1226 - Comeselle, A. L., & Urgeles, R. (2017). Large-scale margin collapse during Messinian early sea-
1227 level drawdown: the SW Valencia trough, NW Mediterranean. *Basin Research*, 29, 576-595.
- 1228 - Capó, A., & Garcia, C. (2019). Basin filling evolution of the central basins of Mallorca since the
1229 Pliocene. *Basin Research*, 31(5), 948-966.
- 1230 - Caruso, A., Pierre, C., Blanc-Valleron, M. M., & Rouchy, J. M. (2015). Carbonate deposition and
1231 diagenesis in evaporitic environments: The evaporative and sulphur-bearing limestones during
1232 the settlement of the Messinian Salinity Crisis in Sicily and Calabria. *Palaeogeography,*
1233 *Palaeoclimatology, Palaeoecology*, 429, 136-162.
- 1234 - Caruso, A., Rouchy, J.M., et al., (2006). The Upper Gypsum unit. In: In: Roveri, M. (Ed.), Post-
1235 Congress FieldTrip of the RCMNS Interim Colloquium (Parma, 2006, *Acta Naturalia de "L'Ateneo*
1236 *Parmense"* 42. pp. 157–168.
- 1237 - Catalano R., Di Stefano, P., Sulli, A. & Vitale, F.P., (1996) - Paleogeography and structure of the
1238 Central Mediterranean: Sicily and its offshore area, *Tectonophysics*, 260, 291-323.

- 1239 - Catalano, R., Valenti, V., Albanese, C., Accaino, F., Sulli, A., Tinivella, U., ... & Giustiniani, M.
1240 (2013). Sicily's fold-thrust belt and slab roll-back: the SI. RI. PRO. seismic crustal
1241 transect. *Journal of the Geological Society*, 170(3), 451-464.
- 1242 - CIESM, (2008). The Messinian salinity crisis from mega-deposits to microbiology. In: Briand, F.
1243 (Ed.), A consensus report, in *33ème CIESM Workshop Monographs*, 33. CIESM, 16, bd de Suisse,
1244 MC-98000, Monaco, pp. 1–168.
- 1245 - Cita, M. B., & Colombo, L. (1979). Sedimentation in the latest Messinian at Capo Rossello (Sicily).
1246 *Sedimentology*, 26(4), 497-522.
- 1247 - Clauzon, G., Suc, J.-P., Gautier, F., Berger, A., Loutre, M.F. (1996). Alternate interpretation of the
1248 Messinian salinity crisis, controversy resolved? *Geology* 24, 363–366.
- 1249 - Clauzon, G., Suc, J.-P., Popescu, S.-M., Marunt, Eanu, M., Rubino, J.-L., Marinescu, F., Melinte,
1250 M.C. (2005). Influence of the Mediterranean sea-level changes over the Dacic Basin (Eastern
1251 Paratethys) in the Late Neogene. The Mediterranean Lago Mare facies deciphered. *Basin*
1252 *Research* 17, 437–462.
- 1253 - Dal Cin, M., Accaino, F., Camerlenghi, A., Del Ben, A., Geletti, R., Mocnik, A., ... & Zgur, F. (2015).
1254 The Messinian salinity crisis in the West-Mediterranean Sea-some previous results about the
1255 Messinian events. In *77th EAGE Conference and Exhibition-Workshops*.
- 1256 - De Lange, G.J., Krijgsman, W. (2010). Messinian salinity crisis: a novel unifying shal-low
1257 gypsum/deep dolomite formation mechanism. *Marine Geology* 275, 273–277.
- 1258 - Decima, A., McKenzie, J.A., Schreiber, B.C. (1988). The origin of “evaporative” limestones: an
1259 example from the Messinian of Sicily (Italy). *J. Sediment. Petrol.* 58, 256–272.
- 1260 - Decima, A., Wezel, F.C. (1971). Osservazioni sulle evaporiti Messiniane della Sicilia
1261 centromeridionale. *Rivista Mineraria Siciliana* 130–134, 172–187.
- 1262 - Decima, A., Wezel, F.C. (1973). Late Miocene evaporites of the central Sicilian basin, Italy. In:
1263 Ryan, W.B.F., Hsü, K.J., et al. (Eds), *Initial Rep. Deep Sea Drill. Prog., vol. 13. U.S. Govt. Printing*
1264 *Office, Washington*, pp. 1234–1240.
- 1265 - Dela Pierre, F., Bernardi, E., Cavagna, S., Clari, P., Gennari, R., Irace, A., Lozar, F., Lugli, S., Manzi,
1266 V., Natalicchio, M., Roveri, M., Violanti, D. (2011). The record of the Messinian salinity crisis in
1267 the Tertiary Piedmont Basin (NW Italy): the Alba section revisited. *Palaeogeography,*
1268 *Palaeoclimatology, Palaeoecology* 310, 238–255.
- 1269 - Driussi, O., Maillard, A., Ochoa, D., Lofi, J., Chanier, F., Gaullier, V., ... & Garcia, M. (2015).
1270 Messinian Salinity Crisis deposits widespread over the Balearic Promontory: Insights from new
1271 high-resolution seismic data. *Marine and Petroleum Geology*, 66, 41-54.
- 1272 - Durand-Delga, M., Freneix, S., Magné, J., Méon, H., Rangheard, Y. (1993). La série saumâtre et
1273 continentale d'âge Miocène moyen et supérieur d'Eivissa (ex-Ibiza, Baléares). *Acta. Geol. Hisp.*
1274 *Barcelona* 28–1, 33–46.
- 1275 - Escutia, C. and Maldonado, A. (1992). Palaeogeographic implications of the Messinian surface in
1276 the Valencia Trough, northwestern Mediterranean Sea. *Tectonophysics*, 203(1-4), pp.263-284.

- 1277 - Esteban, M. (1979). Significance of the Upper Miocene coral reefs of the western
1278 Mediterranean. *Palaeogeography, Palaeoclimatology, Palaeoecology* 29, 169-188.
- 1279 - Feng, Y.E., Yankelzon, A., Steinberg, J., Reshef, M. (2016). Lithology and characteristics of the
1280 Messinian evaporite sequence of the deep Levant Basin, eastern Mediterranean. *Mar. Geol.* 376,
1281 118–131.
- 1282 - García-Veigas, J., Ortí, F.J., Rosell, L., Ayora, C., Rouchy, J.M., Lugli, S. (1995). The Messinian salt
1283 of the Mediterranean: geochemical study of the salt from the central Sicily basin and
1284 comparison with the Lorca Basin (Spain). *Bull. Soc. Géol. Fr.* 166, 699–710.
- 1285 - García-Veigas, J., Cendón, D. I., Gibert, L., Lowenstein, T. K., & Artiaga, D. (2018). Geochemical
1286 indicators in Western Mediterranean Messinian evaporites: Implications for the salinity crisis.
1287 *Marine Geology*, 403, 197-214.
- 1288 - Gelabert, B., Sàbat, F., Rodríguez-Perea, A. (1992). A structural outline of the Serra the
1289 Tramontana of Majorca (Balearic Islands). *Tectonophysics* 203, 167–183.
- 1290 - Ghielmi, M., Minervini, M., Nini, C., Rogledi, S., & Rossi, M. (2013). Late Miocene-Middle
1291 Pleistocene sequences in the Po Plain-Northern Adriatic Sea (Italy): the stratigraphic record of
1292 modification phases affecting a complex foreland basin. *Marine and Petroleum Geology*, 42, 50-
1293 81. Grasso M. & Butler R. W. H. (1991) - Tectonic controls on the deposition of late Tortonian
1294 sediments in the Caltanissetta Basin of central Sicily. *Mem. Soc. Geol. Ital.*, 47, 313-324.
- 1295 - Grossi, F., Gliozzi, E., Anadon, P., Castorina, F., & Voltaggio, M. (2015). Is *Cyprideis agrigentina*
1296 *Decima* a good paleosalinometer for the Messinian Salinity Crisis? Morphometrical and
1297 geochemical analyses from the Eraclea Minoa section (Sicily). *Palaeogeography,*
1298 *Palaeoclimatology, Palaeoecology*, 419, 75-89.
- 1299 - Gvirtzman, Z., Manzi, V., Calvo, R., Gavrieli, I., Gennari, R., Lugli, S., ... & Roveri, M. (2017). Intra-
1300 Messinian truncation surface in the Levant Basin explained by subaqueous dissolution. *Geology*,
1301 45(10), 915-918.
- 1302 - Gvirtzman, Z., Reshef, M., Buch-Leviatan, O. and Ben-Avraham, Z. (2013). Intense salt
1303 deformation in the Levant Basin in the middle of the Messinian Salinity Crisis. *Earth and*
1304 *Planetary Science Letters*, 379, pp.108-119.
- 1305 - Haq, B., Gorini, C., Baur, J., Moneron, J., Rubino, J.L., (2020). Deep Mediterranean's Messinian
1306 Evaporite Giant: How much salt?. *Global and Planetary Change*, 184, p.103052.
- 1307 - Henriquet, M., Dominguez, S., Barreca, G., Malavieille, J., & Monaco, C. (2020). Structural and
1308 tectono-stratigraphic review of the Sicilian orogen and new insights from analogue modeling.
1309 *Earth-Science Reviews*, 103257.
- 1310 - Hovland, M. (2008). Deep-water coral reefs: Unique biodiversity hot-spots. *Springer Science &*
1311 *Business Media*.
- 1312 - Hsü, K., Ryan, W.B.F., Cita, M. (1973a). Late Miocene desiccation of the Mediterranean. *Nature*
1313 242, 240.
- 1314 - Hsü, K.J., Cita, M.B., Ryan, W.B.F. (1973b). The origin of the Mediterranean evaporites. In:
1315 Ryan, W.B.F., Hsü, K.J., Cita, M.B. (Eds.), *Initial Reports of the Deep Sea Drilling Project* 13, Part 2.
1316 U.S. Government Printing Office, Washington D.C., pp. 1203–1231.

- 1317 - Hsü, K.J., Montadert, L., Bernoulli, D., Cita, M.B., Erikson, A., Garrison, R.E., Kidd, R.B., Melieres,
1318 F., Muller, C., Wright, R.H. (1978). *Initial report of Deep Sea Drilling Project*. Mediterranean Sea,
1319 42. U.S. Government Printing Office, Washington, DC.
- 1320 - Hübscher, C., Tahchi, E., I. Klauke, Maillard, A. and Sahling, H. (2009). Plate and salt tectonic
1321 control of fluid dynamics in the Latakia and Cyprus Basin, eastern Mediterranean.
1322 *Tectonophysics* 470, 173–182.
- 1323 - IGME (Date accessed/Publication date). BDMIN. Base de Datos de Recursos minerales ©*Instituto*
1324 *Geológico y Minero de España (IGME)*. Retrieved from: <http://doc.igme.es/bdmin/>.
- 1325 - ISPRA – Istituto Superiore per la Protezione e la Ricerca Ambientale. *Carta Geologica D’Italia*,
1326 1:50000, Foglio 631. http://www.artasicilia.eu/old_site/web/carg/index.html.
- 1327 - Kastens K.A., J. Mascle, C. Auroux, E. Bonatti, C. Broglia, J. Channell, P. Curzi, K. Emeis, G. Glacon,
1328 S. Hasegawa, W. Hieke, G. Mascle, F. McCoy, J. McKenzie, J. Mendelson, C. Muller, J.-P. Rehault,
1329 A. Robertson, R. Sartori, R. Sprovieri & M. Torii (1988) - ODP Leg 107 in the Tyrrhenian Sea:
1330 Insights into Passive Margin and Back-arc basin evolution, *Geol. Soc. Amer. Bull.*, v. 100, p. 1140-
1331 1156.
- 1332 - Kirkham, C., Bertoni, C., Cartwright, J., Lensky, N. G., Sirota, I., Rodriguez, K., & Hodgson, N.
1333 (2020). The demise of a ‘salt giant’ driven by uplift and thermal dissolution. *Earth and Planetary*
1334 *Science Letters*, 531, 115933.
- 1335 - Krijgsman, W., Fortuin, A. R., Hilgen, F. J., & Sierro, F. J. (2001). Astrochronology for the
1336 Messinian Sorbas Basin (SE Spain) and orbital (precessional) forcing evaporite cyclicity.
1337 *Sedimentary Geology*, 140, 43–60.
- 1338 - Krijgsman, W., Hilgen, F. J., Raffi, I., Sierro, F. J., & Wilson, D. S. (1999b). Chronology, causes and
1339 progression of the Messinian salinity crisis. *Nature*, 400(6745), 652.
- 1340 - Krijgsman, W., Hilgen, F.J., Marabini, S., Vai, G.B. (1999a). New paleomagnetic and
1341 cyclostratigraphic age constraints on the Messinian of the Northern Apennines (Vena del Gesso
1342 Basin, Italy). *Memorie della Società Geologica Italiana* 54, 25–33.
- 1343 - Lezin C., Maillard A., Odonne F., Colinet G., Chanier F. and Gaullier V. (2017). Tectono-
1344 sedimentary evolution of the Miocene-Pliocene series of Ibiza: new onshore evidence of the
1345 Messinian Salinity Crisis. *IAS Octobre 2017 Toulouse*.
- 1346 - Lickorish W.H., Grasso M., Butler R., Argnani A. & Maniscalco R. (1999) - Structural styles and
1347 regional tectonic setting of the “Gela Nappe” and frontal part of the Maghrebian thrust belt in
1348 Sicily. *Tectonics*, 18, 4, 655-668.
- 1349 - Lofi J. (2018). Seismic atlas of the Messinian Salinity Crisis markers in the Mediterranean Sea.
1350 Volume 2 – *Mem. Soc. Geol. fr.*, n.s., 2018, t. 181, and Commission of the Geological Map of the
1351 World, 72p, doi 10.10682/2018MESSINV2.
- 1352 - Lofi, J., Déverchère, J., Gaullier, V., Gillet, H., Gorini, C., Guennoc, P., Loncke, L., Maillard, A.,
1353 Sage, F., Thion, I. (2011a). Seismic atlas of the “Messinian Salinity Crisis” markers in the
1354 Mediterranean and Black seas. *Commission for the Geological Map of the World and Memoires*
1355 *de la Société Géologique de France, Nouvelle Série*, p. 72.

- 1356 - Lofi, J., Gorini, C., Berné, S., Clauzon, G., Tadeu Dos Reis, A., Ryan, W.B.F., Steckler, M. (2005).
1357 Erosional processes and paleo-environmental changes in the Western Gulf of Lions (SW France)
1358 during the Messinian Salinity Crisis. *Marine Geology* 217, 1–30.
- 1359 - Lofi, J., Sage, F., Déverchère, J., Loncke, L., Maillard, A., Gaullier, V., ... & Gorini, C. (2011b).
1360 Refining our knowledge of the Messinian salinity crisis records in the offshore domain through
1361 multi-site seismic analysis. *Bulletin de la Société géologique de France*, 182(2), 163-180.
- 1362 - Londeix, L., Benzakour, M., De Vernal, A., Turon, J. L., & Suc, J. P. (1999). Late Neogene
1363 dinoflagellate cyst assemblages from the Strait of Sicily, Central Mediterranean Sea:
1364 paleoecological and biostratigraphical implications. *The Pliocene: time of change*, 65-91.
- 1365 - Londeix, L., Benzakour, M., Suc, J. P., & Turon, J. L. (2007). Messinian palaeoenvironments and
1366 hydrology in Sicily (Italy): the dinoflagellate cyst record. *Geobios*, 40(3), 233-250.
- 1367 - Lüdmann, T., Wiggershaus, S., Betzler, C., & Hübscher, C. (2012). Southwest Mallorca Island: a
1368 cool-water carbonate margin dominated by drift deposition associated with giant mass
1369 wasting. *Marine Geology*, 307, 73-87.
- 1370 - Lugli, S., Manzi, V., Roveri, M., Schreiber, B.C. (2010). The Primary Lower Gypsum in the
1371 Mediterranean: a new facies interpretation for the first stage of the Messinian salinity crisis.
1372 *Palaeogeography, Palaeoclimatology, Palaeoecology* 297, 83–99.
- 1373 - Lugli, S., Schreiber, B. C., & Triberti, B. (1999). Giant polygons in the Realmonte Mine (Agrigento,
1374 Sicily); evidence for the desiccation of a Messinian halite basin. *Journal of Sedimentary
1375 Research*, 69(3), 764-771.
- 1376 - Lymer, G., Lofi, J., Gaullier, V., Maillard, A., Thion, I., Sage, F., ... & Vendeville, B. C. (2018). The
1377 Western Tyrrhenian Sea revisited: New evidence for a rifted basin during the Messinian Salinity
1378 Crisis. *Marine Geology*, 398, 1-21.
- 1379 - Madof, A. S., Bertoni, C., & Lofi, J. (2019). Discovery of vast fluvial deposits provides evidence for
1380 drawdown during the late Miocene Messinian salinity crisis. *Geology*, 47(2), 171-174.
- 1381 - Maillard A., Gaullier V., Lézin C., Chanier F., Odonne F. and Lofi J. (2020). New onshore/offshore
1382 evidence of the Messinian Erosion Surface from key areas: The Ibiza-Balearic Promontory and
1383 the Orosei-Eastern Sardinian margin. *BSGF Earth Science Bull.* 191, 9.
- 1384 - Maillard, A., & Mauffret, A. (2006). Relationship between erosion surfaces and the Late Miocene
1385 Salinity Crisis deposits in the Valencia Basin (Northwestern Mediterranean): evidence for an
1386 early sea-level drop. *Terra Nova*, 18, 321-329.
- 1387 - Maillard, A., Driussi, O., Lofi, J., Briais, A., Chanier, F., Hübscher, C., & Gaullier, V. (2014). Record
1388 of the Messinian salinity crisis in the SW Mallorca area (Balearic Promontory, Spain). *Marine
1389 Geology*, 357, 304-320.
- 1390 - Maillard, A., Gorini, C., Mauffret, A., Sage, F., Lofi, J., & Gaullier, V. (2006). Offshore evidence of
1391 polyphase erosion in the Valencia Basin (Northwestern Mediterranean): scenario for the
1392 Messinian Salinity Crisis. *Sedimentary Geology*, 188, 69-91.
- 1393 - MAILLARD-LENOIR Agnès, GAULLIER Virginie (2013) SIMBAD cruise, RV Téthys II,
1394 <https://doi.org/10.17600/13450010>.

- 1395 - Manzi, V., Gennari, R., Hilgen, F., Krijgsman, W., Lugli, S., Roveri, M., & Sierro, F. J. (2013). Age
1396 refinement of the Messinian salinity crisis onset in the Mediterranean. *Terra Nova*, 25(4), 315-
1397 322.
- 1398 - Manzi, V., Gennari, R., Lugli, S., Persico, D., Reghizzi, M., Roveri, M., Schreiber, B.C., Calvo, R.,
1399 Gavrieli, I., Gvirtzman, Z. (2018). The onset of the Messinian salinity crisis in the deep Eastern
1400 Mediterranean basin. *Terra Nova* 30, 189–198.
- 1401 - Manzi, V., Gennari, R., Lugli, S., Roveri, M., Scafetta, N., & Schreiber, B. C. (2012). High-frequency
1402 cyclicity in the Mediterranean Messinian evaporites: evidence for solar–lunar climate forcing.
1403 *Journal of Sedimentary Research*, 82(12), 991-1005.
- 1404 - Manzi, V., Lugli, S., Roveri, M., & Charlotte Schreiber, B. (2009). A new facies model for the
1405 Upper Gypsum of Sicily (Italy): chronological and palaeoenvironmental constraints for the
1406 Messinian salinity crisis in the Mediterranean. *Sedimentology*, 56(7), 1937-1960.
- 1407 - Manzi, V., Lugli, S., Roveri, M., Dela Pierre, F., Gennari, R., Lozar, F., ... & Turco, E. (2016). The
1408 Messinian salinity crisis in Cyprus: a further step towards a new stratigraphic framework for
1409 Eastern Mediterranean. *Basin Research*, 28(2), 207-236.
- 1410 - Manzi, V., Lugli, S., Roveri, M., Schreiber, B.C., Gennari, R., (2011). The Messinian CdB (Sicily,
1411 Italy) revisited. *Geol. Soc. Am. Bull.* 123, 347–370.
- 1412 - Mas Gornals, G.Y., Fornós Astó, J.J. (2012). La Crisis de Salinidad del Messiniense en la cuenca
1413 sedimentaria de Palma (Mallorca, Islas Baleares); The Messinian Salinity Crisis Record in the
1414 Palma basin (Mallorca, Balearic Islands). *Geogaceta* 52, 57–60.
- 1415 - Mas, G., Fornós, J.J. (2013). Late Messinian Lago Mare deposits of the island of Mallorca
1416 (Western Mediterranean). Implications on the MSC events. In: Neogene to Quaternary
1417 geological evolution of Mediterranean, Paratethys and Black Sea. *Abstracts book. 14th RCMNS*
1418 *Congress, 8-12 September 2013, Istanbul. Turkey.* p. 210.
- 1419 - Mascle, G. & Mascle, J., (2019). The Messinian salinity legacy: 50 years later. *Mediterranean*
1420 *Geoscience Reviews*, 1-11.
- 1421 - Meilijson, A., Hilgen, F., Sepúlveda, J., Steinberg, J., Fairbank, V., Flecker, R., Wald-mann, N.D.,
1422 Spaulding, S.A., Bialik, O.M., Boudinot, F.G. (2019). Chronology with a pinch of salt: integrated
1423 stratigraphy of Messinian evaporites in the deep East-ern Mediterranean reveals long-lasting
1424 halite deposition during Atlantic connectivity. *Earth-Sci. Rev.*
- 1425 - Mitchum Jr, R. M., & Vail, P. R. (1977). Seismic Stratigraphy and Global Changes of Sea Level:
1426 Part 7. Seismic Stratigraphic Interpretation Procedure: Section 2. Application of Seismic
1427 Reflection Configuration to Stratigraphic Interpretation.
- 1428 - Montadert L., Sancho J., Fial J.-P. & Debysser J. (1970). – De l'âge tertiaire de la série salifère
1429 responsable des structures diapiriques en Méditerranée occidentale (Nord-Est des Baléares). –
1430 *C.R. Acad. Sci., Paris*, 271, 812-815.
- 1431 - Ochoa, D., Sierro, F. J., Hilgen, F. J., Cortina, A., Lofi, J., Kouwenhoven, T., & Flores, J. A. (2018).
1432 Origin and implications of orbital-induced sedimentary cyclicity in Pliocene well-logs of the
1433 Western Mediterranean. *Marine Geology*, 403, 150-164.

- 1434 - Ochoa, D., Sierro, F. J., Lofi, J., Maillard, A., Flores, J. A., & Suárez, M. (2015). Synchronous onset
1435 of the Messinian evaporite precipitation: First Mediterranean offshore evidence. *Earth and*
1436 *Planetary Science Letters*, 427, 112-124.
- 1437 - Odone F., Maillard A., Lézin C., Chanier F., Gaullier V. and Guillaume D. (2019). Large-scale
1438 boudinage of Late Miocene platform series triggered by margin collapse during the Messinian
1439 Salinity Crisis (Ibiza Island, Spain). *Marine and Petroleum Geology*, 109, 852-867.
- 1440 - Ogniben, L. (1957). Petrografia della Serie Solfifera Siciliana e considerazioni geologiche relative.
1441 Mem. Descrit. *Carta Geol. Ital.* 33 (275 pp.).
- 1442 - Pedley, H.M., Maniscalco (1999). Lithofacies and faunal succession (faunal phase analysis) as a
1443 tool on unravelling climatic and tectonic signals in marginal basins; Messinian (Miocene), Sicily.
1444 *J. Geol. Soc. Lond.* 156, 855–863.
- 1445 - Pellen, R., Aslanian, D., Rabineau, M., Suc, j., Gorini, C., Leroux, E., ... & Rubino, J. L. (2019). The
1446 Messinian Ebro River Incision. *Global and Planetary Change*, 181, 102988.
- 1447 - Perri, E., Gindre-Chanu, L., Caruso, A., Cefalà, M., Scopelliti, G., & Tucker, M. (2017). Microbial-
1448 mediated pre-salt carbonate deposition during the Messinian salinity crisis (Calcare di Base fm.,
1449 Southern Italy). *Marine and Petroleum Geology*, 88, 235-250.
- 1450 - Pierre, C., Caruso, A., Blanc-Valleron, M. M., Rouchy, J. M., & Orzsag-Sperber, F. (2006).
1451 Reconstruction of the paleoenvironmental changes around the Miocene–Pliocene boundary
1452 along a West–East transect across the Mediterranean. *Sedimentary Geology*, 188, 319-340.
- 1453 - Pomar, L., Ward, W.C., Green, D.G. (1996). Upper Miocene Reef Complex of the Lluçmajor area,
1454 Mallorca, Spain.). In: Franseen, E., Esteban, M., Ward, W.C., Rouchy, J.M. (Eds.), Models for
1455 Carbonate Stratigraphy from Miocene Reef Complexes of Mediterranean Regions. Soc. Econ.
1456 Paleontol. Mineral., *Concepts in Sedimentology and Palaeontology Serie*, vol. 5, pp. 191–225.
- 1457 - Roca, E. (2001). The Northwest-Mediterranean basin (Valencia Trough, Gulf of Lions and Liguro-
1458 Provençal basins): structure and geodynamic evolution. In: Ziegler, P.A., Cavazza, W., Robertson,
1459 A.F.H. (Eds.), Peri-tethysmemoir, IGCP 369: Peri Tethyan Rift/ Wrench Basins and Passive
1460 Margins. Mem. *Mus. Natl. Hist. Nat.*, pp. 671–706 (Paris).
- 1461 - Roca, E., Guimera, J. (1992). The Neogene structure of the Eastern Iberian margin: structural
1462 constraints on the crustal evolution of the Valencia Trough (Western Mediterranean).
1463 *Tectonophysics* 203, 203–218.
- 1464 - Rosell, L., Orti, F., Kasprzyk, A., Playà, E., Marek Peryt, T. (1998). Strontium geochemistry of
1465 Miocene primary gypsum: Messinian of Southeastern Spain and Sicily and Badenian of Poland.
1466 *Journal of Sedimentary Research* 68, 63–79.
- 1467 - Rouchy, J. M., & Caruso, A. (2006). The Messinian salinity crisis in the Mediterranean basin: a
1468 reassessment of the data and an integrated scenario. *Sedimentary Geology*, 188, 35-67.
- 1469 - Rouchy, J.M. (1976). Mise en évidence de nannoplancton calcaire dans certains types de gypse
1470 finement lité (balatino) du Miocène terminal de Sicile et conséquences sur la genèse des
1471 évaporites méditerranéennes de cet âge. *C. R. Acad. Sci. Paris* 282, 13–16.
- 1472 - Rouchy, J.M. (1982a). La genèse des évaporites messiniennes de Méditerranée. *Bulletin du*
1473 *Muséum National d'Histoire Naturelle Paris, Science de la Terre*, pp. 1–280.

- 1474 - Rouchy, J.-M., and Saint-Martin, J.-P. (1992), Late Miocene events in the Mediterranean as
1475 recorded by carbonate-evaporite relations: *Geology*, v. 20, p. 629– 632.
- 1476 - Roveri, M., Bassetti, M. A., & Ricci Lucchi, F. (2001). The Mediterranean messinian salinity crisis:
1477 An Apennine foredeep perspective. *Sedimentary Geology*, 140, 201–214.
- 1478 - Roveri, M., Flecker, R., Krijgsman, W., Lofi, J., Lugli, S., Manzi, V., ... & Govers, R. (2014a). The
1479 Messinian Salinity Crisis: past and future of a great challenge for marine sciences. *Marine
1480 Geology*, 352, 25-58.
- 1481 - Roveri, M., Gennari, R., Ligi, M., Lugli, S., Manzi, V., & Reghizzi, M. (2019). The synthetic seismic
1482 expression of the Messinian salinity crisis from onshore records: Implications for shallow-to
1483 deep-water correlations. *Basin Research*, 31(6), 1121-1152.
- 1484 - Roveri, M., Lugli, S., Manzi, V., & Schreiber, B. C. (2008). The shallow-to deep-water record of
1485 the Messinian salinity crisis: new insights from Sicily, Calabria and Apennine basins. In *CIESM
1486 Workshop Monographs* (Vol. 33, pp. 73-82).
- 1487 - Roveri, M., Lugli, S., Manzi, V., Gennari, R., & Schreiber, B. C. (2014b). High-resolution strontium
1488 isotope stratigraphy of the Messinian deep Mediterranean basins: Implications for marginal to
1489 central basins correlation. *Marine Geology*, 349, 113-125.
- 1490 - Roveri, M., Manzi, V., Lugli, S., Schreiber, B.C., Caruso, A., Rouchy, J.-M., Iaccarino, S.M.,
1491 Gennari, R., Vitale, F.P., Ricci Lucchi, F., (2006). Clastic vs. primary precipitated evaporites in the
1492 Messinian Sicilian basins. *RCMNS IC Parma 2006 "The Messinian Salinity Crisis Revisited II" Post-
1493 Congress field-trip. Acta Naturalia de "L'Ateneo Parmense"* 42-4, 125–199.
- 1494 - Ruf, A. S., Simo, J. T., & Hughes, T. M. (2012). Insights on Oligocene-Miocene carbonate mound
1495 morphology and evolution from 3D seismic data, East Java Basin, Indonesia. *AAPG Annual
1496 Meeting, Long Beach, California, April 1-4, 2007, AAPG©2012.*
- 1497 - Ryan, W. B. (1976). Quantitative evaluation of the depth of the western Mediterranean before,
1498 during and after the Late Miocene salinity crisis. *Sedimentology*, 23(6), 791-813.
- 1499 - Ryan, W. B. (1978). Messinian badlands on the southeastern margin of the Mediterranean Sea.
1500 *Marine Geology*, 27(3-4), 349-363.
- 1501 - Ryan, W. B. (2009). Decoding the Mediterranean salinity crisis. *Sedimentology*, 56(1), 95-136.
- 1502 - Ryan, W.B.F., Stanley, D.J., Hersey, J.B., Fahlquist, D.A., Allan, T.D., (1971). The tectonics and
1503 geology of the Mediterranean Sea. In: Maxwell, A.E. (Ed.), *The Sea. Wiley-Interscience, New
1504 York*, pp. 387–492.
- 1505 - Sabat, F., Gelabert, B., Rodriguez-Perea, A., Giménez, J. (2011). Geological structure and
1506 evolution of Majorca: implications for the origin of the Western Mediterranean. *Tectonophysics*
1507 510, 217–238.
- 1508 - Samperi, L., Giorgio, M., Kamaldeen, O., Alba, Z., Nicolas, W., Sabrina, N., ... & Francesco, B.
1509 (2020). Estimation of the physical, petrophysical and mineralogical properties of Messinian salt
1510 rocks, Sicily: Implications for multidisciplinary applications. *Marine and Petroleum Geology*, 112,
1511 104032.
- 1512 - Schreiber, B.C. (1978). Environments of subaqueous gypsum deposition. In: Dean, E., Schreiber,
1513 B.C. (Eds.), *Marine Evaporites. SEPM Short Course*, vol. 4, pp. 43–73.

- 1514 - Schreiber, B.C., Friedman, G.M., Decima, A., Schreiber, E. (1976). Depositional environments of
1515 Upper Miocene (Messinian) evaporite deposits of the Sicilian Basin. *Sedimentology* 23, 729–760.
- 1516 - Selli, R. (1960). *Il Messiniano Mayer-Eymar 1867: Proposta di un neostratotipo*. Museo
1517 Geologico "Giovanni Capellini".
- 1518 - Servicio WMS GEODE. Mapa Geológico Continuo de España a escala 1:50.000 @*Instituto*
1519 *Geológico y Minero de España (IGME)* (Date accessed). Retrieved from:
1520 http://mapas.igme.es/gis/services/Cartografia_Geologica/IGME_Geode_50/MapServer/WMSServer
- 1521 - Soria, J.M., Caracuel, J.E., Corbí, H., Dinarès-Turell, J., Lancis, C., Tent-Manclús, J.E., Viseras, C.,
1522 Yébenes, A. (2008). The Messinian–early Pliocene stratigraphic record in the southern Bajo
1523 Segura Basin (Betic Cordillera, Spain): implications for the Mediterranean salinity crisis.
1524 *Sediment. Geol.* 203, 267–288.
- 1525 - Suc, J.-P., Violanti, D., Londeix, L., Poumot, C., Robert, C., Clauzon, G., Gautier, F., Turon, J.L.,
1526 Ferrier, J., Chikhi, H., Cambon, G. (1995a). Evolution of the Messinian Mediterranean
1527 environments: the Tripoli Formation at Capodarso (Sicily, Italy). *Review of Palaeobotany and*
1528 *Palynology* 87, 51–79.
- 1529 - Thinon, I., Guennoc, P., Serrano, O., Maillard, A., Lasseur, E., & Rehault, J. P. (2016). Seismic
1530 markers of the Messinian Salinity Crisis in an intermediate-depth basin: data for understanding
1531 the Neogene evolution of the Corsica Basin (Northern Tyrrhenian Sea). *Marine and Petroleum*
1532 *Geology*, 77, 1274-1296.
- 1533 - Urgeles, R., Camerlenghi, A., Garcia-Castellanos, D., De Mol, B., Garcés, M., Vergés, J., ... &
1534 Hardman, M. (2011). New constraints on the Messinian sealevel drawdown from 3D seismic
1535 data of the Ebro Margin, western Mediterranean. *Basin Research*, 23(2), 123-145.
- 1536 - Vai, G. B., & Lucchi, F. R. (1977). Algal crusts, autochthonous and clastic gypsum in a cannibalistic
1537 evaporite basin: a case history from the Messinian of Northern Apennines. *Sedimentology*,
1538 24(2), 211-244.
- 1539 - Van Couvering, J. A., Castradori, D., Cita, M. B., Hilgen, F. J., & Rio, D. (2000). The base of the
1540 Zanclean Stage and of the Pliocene Series. *Episodes*, 23(3), 179-187.
- 1541 - Warren, J. K. (2016). *Evaporites: A geological compendium*. Springer.
- 1542 - Ziegenbalg, S.B., Brunner, B., Rouchy, J.M., Birgel, D., Pierre, C., Böttcher, M.E., Caruso, A.,
1543 Immenhauser, A., Peckmann, J. (2010). Formation of secondary carbonates and native sulphur in
1544 sulphate-rich Messinian strata, Sicily. *Sediment. Geol.* 227, 37–50.